

NASA TECHNICAL NOTE



NASA TN D-5376

NASA TN D-5376

# CASE FILE COPY

OXIDATION AND THERMAL FATIGUE  
CRACKING OF NICKEL- AND COBALT-BASE  
ALLOYS IN A HIGH VELOCITY GAS STREAM

*by James R. Johnston and Richard L. Ashbrook*

*Lewis Research Center*

*Cleveland, Ohio*

NATIONAL AERONAUTICS AND SPACE ADMINISTRATION • WASHINGTON, D. C. • AUGUST 1969

OXIDATION AND THERMAL FATIGUE CRACKING OF NICKEL- AND  
COBALT-BASE ALLOYS IN A HIGH VELOCITY GAS STREAM

By James R. Johnston and Richard L. Ashbrook

Lewis Research Center  
Cleveland, Ohio

NATIONAL AERONAUTICS AND SPACE ADMINISTRATION

#### ABSTRACT

The superalloys IN-100, B-1900, Mar M-200, TAZ3A, Hastelloy X, TD-NiCr, L-605, X-40, Mar M-509A, and WI-52 were cyclically tested for resistance to oxidation in high velocity gas streams for 100 cycles between room temperature and temperatures up to 2000<sup>0</sup> F (1093<sup>0</sup> C). Conventionally cast nickel-base alloys were more resistant to weight loss than cast cobalt-base alloys, but cast cobalt-base alloys were more resistant to thermal fatigue cracking. However, Hastelloy X and directionally solidified and single grain Mar M-200 did not crack even after 100 cycles to 2000<sup>0</sup> F (1093<sup>0</sup> C). Simulated steady-state conditions reduced weight loss and incidence of cracking of the six alloys so tested.

# OXIDATION AND THERMAL FATIGUE CRACKING OF NICKEL- AND COBALT-BASE ALLOYS IN A HIGH VELOCITY GAS STREAM

by James R. Johnston and Richard L. Ashbrook

Lewis Research Center

## SUMMARY

An investigation was conducted to determine the resistance to oxidation of typical gas turbine alloys exposed alternately to high and low temperature, high velocity gas streams. A natural gas-compressed air burner was used to produce velocities up to Mach 1 and specimen temperatures up to  $2000^{\circ}\text{F}$  ( $1093^{\circ}\text{C}$ ). The materials tested included six nickel-base alloys: IN-100, B-1900, Mar M-200, TAZ-8A, Hastelloy X, and TD-NiCr, and four cobalt-base alloys: L-605, X-40, Mar M-509A, and WI-52.

In a standard test of 100 cycles of 1 hour at temperature in a Mach 1 gas stream followed by rapid cooling to room temperature, the nickel-base alloys as a class experienced less weight loss than the cobalt-base alloys. The average values of weight loss varied widely from 216 to 23 700 milligrams after 100 hours at  $2000^{\circ}\text{F}$  ( $1093^{\circ}\text{C}$ ). Of the cobalt-base alloys, X-40 had the lowest weight loss, which was only slightly less than that of Mar M-200. The latter alloy had the highest weight loss of all of the nickel alloys. Of all the alloys tested, the cast cobalt-base alloy, WI-52, was the least resistant to weight loss. After 100 hours, surface recession paralleled weight loss and ranged from 0.3 to 50 mils (0.008 to 1.3 mm).

Cast cobalt-base alloys were more resistant to thermal fatigue cracking than conventionally cast nickel-base alloys. However, directionally solidified and single grain Mar M-200 castings and wrought Hastelloy X had no cracks even after 100 cycles at  $2000^{\circ}\text{F}$  ( $1093^{\circ}\text{C}$ ).

At  $2000^{\circ}\text{F}$  ( $1093^{\circ}\text{C}$ ) under simulated steady-state operation (10-hour cycles with free air cooling to room temperature) the average weight loss was less for the six alloys so tested than at standard conditions. Cobalt alloys showed more improvement in oxidation resistance from the change in cycle than the nickel-base alloys. No cracking was observed in any alloy under these conditions. When the lower temperature during a  $2000^{\circ}\text{F}$  ( $1093^{\circ}\text{C}$ ) test was restricted to  $1200^{\circ}\text{F}$  ( $649^{\circ}\text{C}$ ), the propensity toward cracking was unchanged for IN-100, and B-1900, but substantially reduced for WI-52. However, weight loss decreased substantially for all alloys so tested.

## INTRODUCTION

The dynamic conditions of oxidation that exist in a gas turbine are very different from the essentially static conditions used in many oxidation studies. The high gas velocities and pressures in an engine increase the heat flux as well as chemical reactivity. The cyclic operation results in thermal stresses that not only cause potentially protective scales to spall, but also cause cracking of the blades or vanes themselves.

Various types of facilities have been used to study oxidation and hot corrosion of turbine alloys and coatings (refs. 1 to 5). Such facilities include modified furnaces with relatively low velocity gas flow (ref. 4) as well as a high pressure flame tunnel (ref. 5). Typical systems, however, use relatively low pressure burners exhausting to atmosphere with jet velocities of Mach 0.5 to 0.8.

In order to study at first hand the behavior of gas turbine materials under conditions which more nearly simulate engine operation conditions than furnace tests run in still air, a test facility was constructed at NASA Lewis Research Center. The facility was designed to expose specimens to a high velocity, high mass flow, high temperature gas stream, and to intermittently expose them to a jet of cold air.

Uncoated specimens of representative commercially available nickel-base and cobalt-base alloys as well as a NASA nickel-base alloy were cyclically tested for times up to 100 hours at temperatures ranging from 1700<sup>o</sup> to 2000<sup>o</sup> F (927<sup>o</sup> to 1093<sup>o</sup> C). These temperatures were achieved with a burner using natural gas. No salt or sulfur was added to the gas stream. At intervals the specimens were removed from the apparatus and weighed, measured and examined for cracks. Representative specimens were examined metallographically, and the oxides present in their scales were determined by X-ray diffraction.

In addition, a limited amount of information was obtained concerning the effects of variations in the operating conditions. The effects of gas velocity and of reducing the temperature spread during cyclic testing, as well as the effect of increasing the time at temperature for each cycle were studied.

## MATERIALS, APPARATUS, AND PROCEDURE

### Specimens

A drawing of the specimen used is shown in figure 1. It was 4 by 1 by 1/4 inches (10.2 by 2.5 by 0.6 cm) tapered along one of the long edges with a 45<sup>o</sup> included angle and a 0.03 inch (0.8 mm) radius to simulate the contour of an airfoil leading or trailing edge. Because the tapered edges of the specimens were outermost in the specimen

holder and came closest to the burner nozzle, as the specimen holder rotated, they will be called the "leading" edges in this report.

## Materials

Conventionally cast alloys. - The majority of the materials tested were investment cast by commercial foundries. Inoculated molds were used to produce a fine grain size typical of that used for gas turbine blades and vanes. Figure 2 shows a macrograph of representative cast specimens etched to reveal their grain structure. The etchant was concentrated hydrochloric acid with enough hydrogen peroxide to produce a vigorous attack of the cast surface. The compositions of the cast alloys as well as the compositions of materials produced by other methods are listed in table I. Four of the conventionally cast materials were nickel base: three commercial alloys IN-100, B-1900, and Mar M-200 and an experimental NASA alloy TAZ-8A (ref. 6). Three were cobalt base: X-40, Mar M-509A, and WI-52.

Wrought alloys. - One wrought cobalt-base alloy, L-605, and one wrought nickel-base alloy, Hastelloy X, were tested. The specimens of both alloys were machined from 5/16-inch (8-mm) thick plate. The long dimension of the specimens was parallel to the rolling direction.

Dispersion strengthened alloy. - The dispersion strengthened nickel-base alloy, TD-NiCr, was also tested. Specimens were machined from 1/4-inch (6-mm) thick plate with the long dimension of the specimens parallel to the major rolling direction of this cross-rolled material.

Since TD-NiCr is normally furnished as sheet rather than as plate, it should be recognized that this material was not as severely worked as regular TD-NiCr.

Controlled macrostructure alloys. - Mar M-200 was tested as conventionally cast and was also tested in two forms produced by controlled solidification. Figure 3 shows all three types of macrostructure. The conventionally cast material had a relatively fine grained equiaxed structure. "Directionally solidified" material had a number of grains running parallel to the long axis of the specimen. The proprietary process used to make these castings is such that the [100] crystallographic direction of the face centered cubic matrix is parallel to the long dimension (growth direction) of the casting.

The single grain castings tested were substantially single grained although a few of the specimens tested had grain boundaries in the base where they were gripped. These single grain castings were also produced by a proprietary method that resulted in grains oriented with the [100] direction parallel to the growth direction (long axis of these specimens).

TABLE I. - CHEMICAL COMPOSITION OF TEST MATERIALS

Alloy	Composition, wt. %															
	Ni	Co	Cr	Mo	W	Cb	Ta	C	Ti	Al	Si	Mn	Fe	B	Zr	Other
IN-100	Bal.	14.91	10.00	2.95	-----	-----	----	0.15	4.34	5.45	0.11	<0.05	0.14	0.015	0.06	V 0.90 S 0.002
B-1900		10.10	7.95	6.07	<0.10	<0.10	4.30	.10	1.00	5.80	.10	<.02	.16	.013	.08	S 0.001
TAZ-8A <sup>a</sup>		-----	5.93	3.70	3.84	2.21	8.02	.15	----	5.70	----	----	-----	.004	.64	-----
TD-NiCr		-----	21.39	----	----	-----	----	.04	----	----	----	----	-----	-----	-----	ThO <sub>2</sub> 2.5
Hastelloy X <sup>b</sup>		1.5	21.75	9.0	.60	-----	----	.10	----	----	<1.0	<1.0	18.5	-----	-----	-----
MAR M-200		10.50	9.17	----	12.65	-----	.99	.14	1.93	4.95	.052	<.02	.21	.017	.053	S 0.006
L-605 <sup>b</sup>	10.0	Bal.	20.0	----	15.0	-----	----	.10	----	----	<1.0	1.5	<3.0	-----	-----	S <.03 P <.03
X-40	10.53		25.56	----	7.57	-----	----	.49	----	----	.38	<.05	.29	-----	-----	S 0.003
MAR M-509A	9.50		23.7	----	6.87	-----	3.36	.58	.20	----	<.1	<.1	.16	<.01	.58	S 0.010
WI-52	.53		21.02	----	11.07	1.89	----	.44	----	----	.29	.28	1.69	-----	-----	P 0.006 S 0.04

<sup>a</sup>Typical (ref. 6).<sup>b</sup>Vendor's nominal.

The end of the controlled structure castings which was nearest the chill was uppermost during testing. Both sets of castings with the controlled macrostructure were heat treated in vacuum at  $2230^{\circ}$  ( $1221^{\circ}$  C) for 2 hours, then aged in air at  $1600^{\circ}$  F ( $871^{\circ}$  C) for 36 hours.

## High Gas-Velocity Cyclic Oxidation Apparatus

The burner installation is shown in figure 4. The photograph indicates the general configuration of the burner and the rotating specimen holder. The schematic diagram also shown in figure 4 depicts the positions of the specimens with respect to the burner exit nozzle and the cooling air nozzle. The specimens were mounted on a rotating fixture that was moved vertically between heating and cooling positions by an air cylinder. In the heating position the specimens were partially surrounded by a segmented cylindrical radiation shield. This shield was used to minimize the span-wise and chord-wise temperature gradients within the specimen. A slip-ring assembly, mounted in the lower end of the specimen holder shaft, was used to provide an electrical circuit to a thermocouple mounted in one of the specimens.

The burner was designed to burn natural gas with compressed air up to approximately 55 psia ( $0.038 \text{ MN/m}^2$ ) with exit gas temperatures as high as  $3000^{\circ}$  F ( $1649^{\circ}$  C). A double liner (not shown) was used to permit the combustion air to efficiently cool the outer jacket as well as the flame tube. Water cooling was used only on the converging exit nozzle. Accordingly, heat losses were minimized and the resulting fuel/air ratio was as lean as possible.

A photograph of the specimen holder is shown in figure 5. The holder has provision for eight specimens which were secured by retaining pins and lock screws. The pin-lock screw method was used to permit machining specimens from rolled stock as thin as 1/4 inch (0.63 cm). A flat radiation shield protected the upper surface of the specimen holder from direct impingement of hot gases as well as radiation from the hot specimens. Additional protection was provided by an air jet directed between the shield and the specimen holder. The use of cooling air on the holder maintained its operating temperatures well below  $1000^{\circ}$  F ( $538^{\circ}$  C) with specimen temperatures as high as  $2000^{\circ}$  F ( $1093^{\circ}$  C). The specimen holders were machined from stainless steel.

The temperature of the rotating specimens was monitored with a chromel-alumel thermocouple (see fig. 6) imbedded in a dummy specimen used in each run, and by an optical pyrometer sighting through the control room window. The burner gas temperature was controlled by using an exhaust gas thermocouple (fig. 4) downstream of the specimens. By controlling the gas temperature the specimen temperature was maintained within  $\pm 15^{\circ}$  F ( $\pm 8^{\circ}$  C) of the nominal test temperature.

Typical axial and chordwise temperature profiles of the specimen are also shown in figure 6. The axial temperatures were measured with an optical pyrometer scanning rotating specimens so that the results were averaged along the chord. The chordwise temperature distribution was measured with thermocouples imbedded in a specimen at the position where the maximum axial temperature was indicated by the optical measurements.

The maximum axial temperature occurred at or close to the centerline of the impinging gas jet. From the maximum temperature zone, the temperature gradually decreased by approximately 75° to 100° F per inch (16° to 22° C/cm). The chordwise temperature profile was essentially linear with the maximum temperature occurring at the trailing edge, about 25° F (14° C) higher than the midchord or nominal test temperature. Conversely, the leading edge temperature was about 25° F (14° C) lower than the midchord temperature.

## Test Conditions

The standard test conditions used for this investigation are shown in table II. The specimens were alternately heated for 1 hour at the specified test temperature and cooled for 3 minutes to room temperature. The cycling was normally continued for 100 hours. The burner chamber pressure was maintained at 33 psia (0.23 MN/m<sup>2</sup>) to assure an exit velocity of Mach 1 at the nozzle throat. The cooling air nozzle exit velocity was also Mach 1.

Several tests were conducted with modified test conditions in order to determine the gross effect of specific parameters. Three modified test conditions were used:

- (1) Standard conditions except Mach 0.7 rather than Mach 1 velocity during heating

TABLE II. - TYPICAL BURNER CONDITIONS FOR STANDARD TESTS

[Specimen test cycle: 1 hr at maximum temperature,  
3-min cool to room temperature.]

Maximum specimen temperature, °F (°C)	1700 to 2000 (927 to 1093)
Burner gas temperature, °F (°C)	2400 to 2800 (1316 to 1538)
Gas velocity	Mach 1
Burner pressure, psia (MN/m <sup>2</sup> )	33 (0.023)
Specimen rotational speed, rpm	900
Burner air flow, lbm/sec (kg/sec)	0.9 to 1.0 (0.41 to 0.45)
Cooling air flow, lbm/sec (kg/sec)	0.5 (0.23)
Air to fuel ratio	20 to 30
Burner nozzle diameter, in. (cm)	2.0 (5.1)

- (2) "Steady-state" operation at Mach 1 velocity with shutdowns occurring approximately every 10 hours. Cooling was without forced air.
- (3) Operation at Mach 1 with modified cooling cycle; rate of cooling was similar to the standard test, but specimens were cooled only to 1200<sup>0</sup> F (649<sup>0</sup> C) before reheating.

Typical heating and cooling curves are shown in figure 7 for the various test cycles. A thermocouple imbedded in a dummy specimen at mid-chord (fig. 6) was used for these measurements. In the standard cycle figures 7(a) and (b), the temperature reached near-equilibrium in about 1 minute on heating and about 1.5 minutes on cooling. The Mach 0.7 heating curve was not appreciably different from that for Mach 1. The reason for this is that a higher gas temperature was required to maintain a given specimen temperature because of the lower heat transfer coefficient at Mach 0.7. The slow cooling curve obtained from the steady-state cycle is shown in figure 7(c). In this cooling mode, that is, without forced air cooling, the specimens required more than 10 minutes to cool to room temperature. The heating and cooling curves for the modified cooling cycle are shown in figure 7(d). The rates are similar to those of the standard test.

## Test Procedure

Prior to testing all specimens were degreased in trichlorethylene vapor and weighed on an analytical balance with a precision of 0.2 mg. At intervals of 20 hours of testing the specimens were removed from the apparatus, reweighed, photographed, and inspected for cracks with fluorescent dye penetrant. Prior to further testing they were again degreased. In most cases, one specimen was removed for metallographic examination after 20 hours and another after 60 hours of testing.

The surface recession of several representative materials was measured using specimens modified as shown in figure 8. Platinum alloy pins approximately 0.05 inch (0.13 cm) in diameter were peened into holes drilled through the specimens at the locations shown. These pins were polished and marked with a Knopp hardness diamond indenter to provide a sharply defined reference mark. Before testing and at each 20-hour inspection period the distances from each reference mark to the leading and trailing edges were measured using an optical comparator having a sensitivity of 0.0005 inch (0.0013 cm) and a repeatability of 0.0001 inch (0.00025 cm).

Specimens of each alloy were sectioned for metallographic examination. Generally, longitudinal and transverse sections were made near the maximum temperature zone of the specimens. Care was taken to cut the longitudinal sections close to the center plane of the specimens so that small thermal fatigue cracks on the leading edge could be

examined. Samples of the surface oxides for X-ray diffraction analyses were usually taken at areas adjacent to the metallographic samples.

## RESULTS AND DISCUSSION

### Standard Cycle

Weight change. - The results of weight change measurements for 10 materials are shown in figure 9. These data were obtained during 100-hour tests with the high gas velocity oxidation apparatus operated with the standard cycle. The curves shown were generated by averaging the data from five to seven specimens. The weight change observed for all alloys was a loss rather than the gain normally observed in static oxidation tests. A summary of these results after 100 hours is shown in figure 10. It is clear that the materials varied widely in performance. For example, after 100 hours at 2000<sup>o</sup> F (1093<sup>o</sup> C), the weight loss of WI-52 was approximately 100 times that of B-1900, IN-100, and TAZ-8A. Even greater differences were noted at lower temperatures. In general, nickel-base alloys showed less weight loss than cobalt-base alloys, although there was some overlapping in performance. The extremes of material loss are shown in figure 11 for B-1900 and WI-52 specimens after 100 hours exposure to the standard cycle with a maximum temperature of 2000<sup>o</sup> F (1093<sup>o</sup> C).

Most of the weight loss curves were relatively linear with time indicating that the protective layer of increasing thickness typical of static oxidation was not formed. Some obvious exceptions to the linear behavior occurred with the 2000<sup>o</sup> F (1093<sup>o</sup> C) curves for Mar M-200 (equiaxed) (fig. 9(f)), several specimens of TAZ-8A (fig. 9(c)), where spalling occurred, and Mar M-509A (fig. 9(i)) where the weight loss rate increased with time. Test specimens of these alloys were characterized by zones of localized spalling at the areas of maximum temperature. As exposure time increased, the zones of spalling enlarged, resulting in an apparent increase in the rate of oxidation.

A comparison of the weight loss results under dynamic conditions with some limited static oxidation data (from the literature) is shown in table III. For the purpose of this comparison, the total weight loss measurements obtained in the burner tests were divided by an area of 30 square centimeters, the estimated area of the specimen over which most of the oxidation occurred. The ratio of weight loss obtained in the high velocity burner tests to the static weight gain varied from 1.3 for IN-100 to 21.2 for WI-52. It is of interest that the differences between alloys are considerably greater in the high velocity tests than in the static tests. This fact and the fact that the ranking of materials is quite different for the two types of tests demonstrates the importance of using dynamic test conditions for evaluating materials for turbine engine applications.

TABLE III. - WEIGHT CHANGES IN HIGH GAS  
VELOCITY-CYCLIC TESTS AND IN STATIC  
OXIDATION TESTS AT 2000° F (1093° C)

Alloy	Test conditions				Absolute ratio of dynamic to static change
	Dynamic weight loss		Static weight gain		
	mg/cm <sup>2</sup> in 50 hr	Rank	mg/cm <sup>2</sup> in 50 hr	Rank	
IN-100	3.7	1	2.8 <sup>(a)</sup>	4	1.3
MAR M-200	10	2	0.9 <sup>(a)</sup>	1	11.1
HASTELLOY X	19.5	4	2.0 <sup>(a)</sup>	3	9.8
TD-NiCr	24	5	1.8 <sup>(b)</sup>	2	13.3
X-40	18	3	4.5 <sup>(a)</sup>	5	4.0
MAR M-509A	46	6	5.0 <sup>(c)</sup>	6	9.2
WI-52	381	7	18 <sup>(a)</sup>	7	21.2

<sup>a</sup>Ref. 9.

<sup>b</sup>Cyclic exposure to 2200° F (1204° C); ref. 10.

<sup>c</sup>Ref. 11.

**Surface recession.** - The results of surface recession measurements are depicted in figure 12 for IN-100, B-1900, TD-NiCr, X-40, Mar M-509A, and WI-52. A summary of surface recession results after 100 hours is shown in figure 13. As in the case of weight loss measurements, the results varied widely between the different alloys. For example, after 100 hours at 2000° F (1093° C) the surface recession of IN-100 was less than 0.5 mil (0.0013 cm) while that of WI-52 was 50 mils (0.13 cm). Except for WI-52 (fig. 12(f)) all materials showed a surface buildup prior to subsequent recession. If inspected sooner than after 20 hours, WI-52 might also have shown a buildup. In several cases, including X-40 (fig. 12(d)) and TD-NiCr (fig. 12(c)), the surface buildup persisted through 60 to 70 hours of testing while at the same time the samples were showing a relatively high weight loss (fig. 9). This anomalous result could possibly be explained by a greater adherence of the scales to edges or curved surfaces than to plane surfaces. Nonetheless, after 100 hours testing, the measured recession at the edges of the specimens was substantially in agreement with a surface recession calculated from weight loss measurements. To obtain a calculated recession, weight loss was normalized over an area of 30 square centimeters where it was assumed that oxidation was actively

occurring. The weight loss per unit area was then divided by the density of the alloy to give the distance the surface had receded. The calculated recession values are plotted in figure 12.

Thermal fatigue cracking. - Summaries of the thermal fatigue results are shown in figures 14(a) and (b) for conventional nickel-base and cobalt-base alloys, respectively. Figure 14(c) depicts the thermal fatigue performance of the controlled solidification Mar M-200 specimens. The incidence of cracking varied widely among the various alloys. Even after 100 hours at 2000<sup>o</sup> F (1093<sup>o</sup> C) no cracks were noted on the wrought nickel-base alloy Hastelloy X nor on the directionally solidified and single grain Mar M-200 specimens. The alloy with the least resistance to cracking was B-1900 (see also fig. 11(a)). Cracks were detected after 40 hours at 1800<sup>o</sup> F (982<sup>o</sup> C) and 20 hours at 1900<sup>o</sup> and 2000<sup>o</sup> F (1038<sup>o</sup> and 1093<sup>o</sup> C). Also, relatively poor in thermal fatigue resistance were Mar M-200 (equiaxed grains), TAZ-8A and IN-100. In general, the cast cobalt alloys were more resistant to thermal fatigue cracking than the cast nickel-base alloys. However, the wrought L-605 specimens were the least crack resistant among the cobalt-base alloys with an incidence of cracking approximately the same as the conventionally cast nickel-base alloys at 1800<sup>o</sup> and 1900<sup>o</sup> F (982<sup>o</sup> and 1038<sup>o</sup> C). L-605 was not tested at 2000<sup>o</sup> F (1093<sup>o</sup> C).

## Effect of Solidification Structure on Weight Loss and Thermal Fatigue

The elimination of transverse grain boundaries has been reported to improve the rupture strength of Mar M-200 (ref. 7). Because of the strength advantages to be gained from controlled solidification structures, a comparison was made of the behavior of castings with the three structures shown in figure 3. More important than the oxidation behavior is the fact that the directionally solidified and single grain castings of Mar M-200 did not crack even after 100 cycles at 2000<sup>o</sup> F (1093<sup>o</sup> C), while the equiaxed castings cracked in 20 cycles or less as shown in figure 14(c).

The oxidation behavior at 2000<sup>o</sup> F (1093<sup>o</sup> C) of the three macrostructures of Mar M-200 is shown in figure 15(a). The equiaxed material was in the as-cast condition while the directionally solidified and single grain material had been heat treated as required by the alloy specifications. The weight losses of the directionally solidified and single grain specimens were practically identical. After 100 hours, they had about five times the weight loss of the equiaxed cast specimens.

Examination of the microstructure of as-received directionally solidified and single grain specimens revealed a recrystallized surface layer depleted of gamma prime precipitate. An example of the structure in a single grain casting is shown in figure 16.

This depleted surface layer was believed to be associated with the presence of oxygen during heat treatment. In order to determine the significance of the depleted zone in affecting the oxidation behavior of these materials, another test was conducted with specimens having approximately 0.01 inch (0.2 mm) machined from the surface to remove the depleted zone. A conventionally cast specimen was also machined to serve as a control.

The oxidation results for the machined specimens are shown in figure 15(b). The weight loss of the machined castings having a controlled structure was still substantially greater than that of the machined equiaxed casting. However, the differences between the weight losses of the controlled structure castings and the equiaxed casting were substantially less than for the unmachined specimens. The reason for the weight loss after machining being greater for the equiaxed specimen and less for the controlled structure specimens may be due to the wide scatter sometimes observed in oxidation tests. Thus, even specimens seemingly identically prepared (for example, the TAZ-8A specimens of this report and L-605 specimens reported elsewhere (ref. 8) can behave differently under nominally identical conditions).

## Metallography

Some of the effects of oxidation under cyclic operation at high gas velocities can be seen from a comparison of the microstructures of the alloys before and after test in figures 17 and 18. Figure 17 shows representative microstructures (magnification, 250) of the as-received test specimens. Figure 18 shows (magnification, 250) the structure at the tapered edge of specimens exposed to cyclic operation for 100 hours at 2000<sup>o</sup> F (1093<sup>o</sup> C). The sections were made at right angles to the long dimension of the specimens near the burner centerline.

The four as-received cast nickel-base alloys IN-100, B-1900, TAZ-8A, and Mar M-200 (conventionally cast) (figs. 17(a), (b), (c), and (f)) had matrices with a fine precipitate of gamma prime. Varying amounts of primary gamma prime were also evident, the largest amount being in TAZ-8A. Interdendritic carbides were also evident, particularly in the commercial alloys IN-100, B-1900, and Mar M-200.

After exposure for 100 hours at 2000<sup>o</sup> F (1093<sup>o</sup> C), these alloys all showed a coarsening of the gamma prime precipitate in the matrix. TAZ-8A showed some coarsening of the primary gamma prime. Directly beneath the oxide scale layers, which were relatively thin except for Mar M-200, were zones of internal oxidation. Both B-1900 and TAZ-8A showed a relatively coarse polygonal oxide constituent in the portion of the depletion zones near the undepleted matrix. These appeared to result from internal oxidation of MC carbides.

The cast cobalt base alloys (figs. 17(i) to (l)) had interdendritic carbide networks in a matrix of solid solution cobalt. Wrought L-605 (fig. 17(i)), which exhibited a recrystallized structure, contained carbides aligned in the direction of rolling. After exposure, the carbides in the cobalt-base alloys (figs. 18(i) to (l)) were somewhat coarsened, and preferential oxidation occurred along carbide networks near the surfaces of the test specimens. L-605 showed considerable precipitation of Laves phase at twin and grain boundaries as has been previously reported (ref. 8).

The advance of the depletion zone with temperature and time in a typical cast nickel-base alloy, B-1900, is shown in figure 19(a).

The advance of interdendritic and internal oxidation in a typical cobalt-base alloy, Mar M-509A, is shown in figure 19(b). At 1800<sup>o</sup> F (982<sup>o</sup> C) the depth of oxide penetration increased with exposure time. For a constant exposure time of 20 hours this oxide penetration increased with temperature. For longer times at higher temperatures it is believed that the intergranular oxides grew together to form a nonadherent continuous scale layer which spalled from the specimen. This would account for the apparent shallower penetration of oxides at 2000<sup>o</sup> F (1093<sup>o</sup> C) in 100 hours than in 20 hours. Scattered particles of internal oxide beneath the surface scale are evident in the micrographs of the specimens exposed at 2000<sup>o</sup> F (1093<sup>o</sup> C) for 60 and 100 hours. The depth of penetration of internal oxidation also increased with time.

TD-NiCr which had been cross rolled showed stringers (fig. 17(d)) both parallel to and perpendicular to the major rolling direction. The burner specimens were all machined with their long dimension parallel to the major rolling direction. Figure 17(d) shows a transverse section through an as-received specimen. The appearance was similar to longitudinal sections cut normal to the plane of the plate. In the plane of the plate no alignment of the thoria dispersoid was evident.

Figure 19(c) shows, at a low magnification, a series of TD-NiCr specimens cyclically tested at 2000<sup>o</sup> F (1093<sup>o</sup> C) for 20, 60, and 100 hours, and for 100 hours at 1800<sup>o</sup>, 1900<sup>o</sup>, and 2000<sup>o</sup> F (982<sup>o</sup>, 1038<sup>o</sup>, and 1093<sup>o</sup> C). The edge at the right of the micrograph represents the nose of the leading edge of the test specimen. The plane of polish is parallel to the largest flat surfaces of the specimens. Microcracks penetrated the specimens at right angles to the edge. The depth of penetration increased with time and temperature. The cracks were filled with oxide and were not revealed by penetrant inspection.

The oxide-filled cracks are intergranular and it is evident in figure 19(c) that they are at right angles to thermal stresses in the edge of the specimen. They are a manifestation of stress-rupture cracking resulting from thermally induced residual stresses and would probably be shown to be interconnected if viewed in three dimensions.

The internal microstructures of the Mar M-200 in the three macrostructures tested were very similar (figs. 17(f) to (h)). However, the surfaces of the columnar and the

single grain castings showed a recrystallized layer about 0.001 inch (25  $\mu\text{m}$ ) thick (fig. 16). This layer, which was depleted in gamma prime, probably was the result of heat treating in an imperfect vacuum, a surface previously worked by sand blasting. However, other forces were also involved because even in the interior of the single grain castings, recrystallization appeared to have occurred in some of the cross shaped dendrite cores as shown in figure 16.

## X-Ray Diffraction

Table IV shows the oxides formed on specimens tested for various times and temperatures. Scrapings for making X-ray diffraction patterns were taken from the tapered portions of the leading edges of the burner specimens near the region of highest axial temperature. Some measurements of the oxide on the specimens before scraping were made with a diffractometer. The results of both methods were essentially the same.

IN-100 and B-1900 behaved in a similar fashion. Both had scales containing alumina ( $\text{Al}_2\text{O}_3$ ) at most of the temperatures and times evaluated. Alumina was missing for IN-100 after 20 hours at  $2000^\circ\text{F}$  ( $1093^\circ\text{C}$ ). The monoxide (probably NiO) was missing for IN-100 only at  $1900^\circ\text{F}$  ( $1038^\circ\text{C}$ ) and 100 hours. It occurred in B-1900 only in the longer times at the highest temperature of  $2000^\circ\text{F}$  ( $1093^\circ\text{C}$ ). Both alloys had spinels at  $2000^\circ\text{F}$  ( $1093^\circ\text{C}$ ). IN-100 formed two spinels, one with a lattice spacing  $a_o$  of  $8.10\text{ \AA}$  ( $8.1 \times 10^{-10}\text{ m}$ ) and one of  $8.30\text{ \AA}$  ( $8.3 \times 10^{-10}\text{ m}$ ). The B-1900 had spinels with spacings of  $8.05$  to  $8.10\text{ \AA}$  ( $8.05$  to  $8.10 \times 10^{-10}\text{ m}$ ).

Although TAZ-8A contains aluminum and chromium neither alumina nor chromia were observed. Except for the specimens tested for 100 hours at  $1800^\circ\text{F}$  ( $982^\circ\text{C}$ ) which had an unidentified oxide X-ray pattern the rest of the TAZ-8A specimens showed only a tri-rutile pattern. Considering the 8 percent tantalum in TAZ-8A, this may indicate the presence of a nickel-tantalate,  $\text{NiTa}_2\text{O}_5$ . If any other oxides were present their patterns were masked by that of tri-rutile.

TD-NiCr was examined for oxides only after 100 hour-test exposure. It is interesting that no chromia was observed, only nickel monoxide, a spinel with an  $a_o$  of  $8.32\text{ \AA}$  ( $8.32 \times 10^{-10}\text{ m}$ ) and thoria. Presumably the chromia sublimed because the high velocity gas stream reduced the local chromia pressure above the specimen surface.

Oxides of Hastelloy X and Mar M-200 were examined also only after 100 hours of testing. A spinel was present in the oxides of both alloys at all of the three test temperatures used. Chromia was present for Hastelloy X at all temperatures and for Mar M-200 at  $1800^\circ\text{F}$  and  $1900^\circ\text{F}$  ( $982^\circ\text{C}$  and  $1038^\circ\text{C}$ ). A monoxide was found only at  $1800^\circ\text{F}$  ( $982^\circ\text{C}$ ) for Hastelloy X and only at  $2000^\circ\text{F}$  ( $1093^\circ\text{C}$ ) for Mar M-200.

TABLE IV. - OXIDES DETERMINED BY X-RAY DIFFRACTION ON MATERIALS EXPOSED TO HIGH-GAS-VELOCITY

OXIDATION APPARATUS FOR VARIOUS TIMES AND TEMPERATURES

Temperature		Time at temperature, hr, and number of cycles			Temperature		Time at temperature, hr, and number of cycles		
°F	°C	20	60	100	°F	°C	20	60	100
		Oxides found					Oxides found		
IN-100					L-605				
1800	982	<sup>a</sup> ND	ND	Al <sub>2</sub> O <sub>3</sub> Monoxide	1800	982	ND	ND	Monoxide <sup>b</sup> Spinel (8.30)
1900	1038	ND	ND	Al <sub>2</sub> O <sub>3</sub> <sup>b</sup> Spinel (8.30)	1900	1038	ND	ND	Monoxide <sup>b</sup> Spinel (8.30)
2000	1093	Monoxide <sup>b</sup> Spinel (8.10) <sup>b</sup> Spinel (8.30)	Al <sub>2</sub> O <sub>3</sub> Monoxide <sup>b</sup> Spinel (8.10) <sup>b</sup> Spinel (8.30)	Al <sub>2</sub> O <sub>3</sub> Monoxide <sup>b</sup> Spinel (8.30)	2000	1093	ND	ND	ND
B-1900					X-40				
1800	982	ND	ND	Al <sub>2</sub> O <sub>3</sub>	1800	982	Cr <sub>2</sub> O <sub>3</sub> <sup>b</sup> Spinel (8.30)	Cr <sub>2</sub> O <sub>3</sub> Spinel (8.30)	Cr <sub>2</sub> O <sub>3</sub>
1900	1038	ND	ND	Al <sub>2</sub> O <sub>3</sub>	1900	1038	Cr <sub>2</sub> O <sub>3</sub> <sup>b</sup> Spinel (8.35)	Cr <sub>2</sub> O <sub>3</sub> Monoxide Spinel CoWO <sub>4</sub>	Cr <sub>2</sub> O <sub>3</sub> Monoxide <sup>b</sup> Spinel (8.35) CoWO <sub>4</sub>
2000	1093	Al <sub>2</sub> O <sub>3</sub> <sup>b</sup> Spinel (8.05)	Al <sub>2</sub> O <sub>3</sub> Monoxide <sup>b</sup> Spinel (8.10)	Al <sub>2</sub> O <sub>3</sub> Monoxide <sup>b</sup> Spinel (8.10)	2000	1093	Cr <sub>2</sub> O <sub>3</sub> Monoxide Spinel	Cr <sub>2</sub> O <sub>3</sub> Monoxide Spinel CoWO <sub>4</sub>	CoO Spinel (8.30)
TAZ-8A					MAR M-509A				
1800	982	<sup>c</sup> Tri-rutile	<sup>c</sup> Tri-rutile	<sup>c</sup> Tri-rutile	1800	982	Cr <sub>2</sub> O <sub>3</sub>	Monoxide <sup>b</sup> Spinel (8.30) CoWO <sub>4</sub>	Cr <sub>2</sub> O <sub>3</sub> Monoxide <sup>b</sup> Spinel (8.30)
1900	1038	<sup>c</sup> Tri-rutile	<sup>c</sup> Tri-rutile	<sup>c</sup> Tri-rutile	1900	1038	Cr <sub>2</sub> O <sub>3</sub> Monoxide <sup>b</sup> Spinel (8.20) <sup>b</sup> Spinel (8.30) CoWO <sub>4</sub>	Cr <sub>2</sub> O <sub>3</sub> Monoxide <sup>b</sup> Spinel (8.15) <sup>b</sup> Spinel (8.30) CoWO <sub>4</sub>	Cr <sub>2</sub> O <sub>3</sub> Monoxide <sup>b</sup> Spinel (8.15) <sup>b</sup> Spinel (8.20) CoWO <sub>4</sub>
2000	1093	<sup>c</sup> Tri-rutile	<sup>c</sup> Tri-rutile	<sup>c</sup> Tri-rutile	2000	1093	Cr <sub>2</sub> O <sub>3</sub> Monoxide <sup>b</sup> Spinel (8.25)	Cr <sub>2</sub> O <sub>3</sub> Monoxide <sup>b</sup> Spinel (8.35) CoWO <sub>4</sub>	Cr <sub>2</sub> O <sub>3</sub> Monoxide <sup>b</sup> Spinel (8.25) CoWO <sub>4</sub>
TD-NiCr					WI-52				
1800	982	ND	ND	Monoxide <sup>b</sup> Spinel (8.32) ThO <sub>2</sub>	1800	982	ND	ND	Cr <sub>2</sub> O <sub>3</sub> Monoxide Spinel CoWO <sub>4</sub>
1900	1038	ND	ND	Monoxide <sup>b</sup> Spinel (8.32) ThO <sub>2</sub>	1900	1038	ND	ND	Cr <sub>2</sub> O <sub>3</sub> Monoxide <sup>b</sup> Spinel (8.30) CoWO <sub>4</sub>
2000	1093	ND	ND	Monoxide <sup>b</sup> Spinel (8.32) ThO <sub>2</sub>	2000	1093	Cr <sub>2</sub> O <sub>3</sub> Monoxide <sup>b</sup> Spinel (8.05) <sup>b</sup> Spinel (8.35) CoWO <sub>4</sub>	Cr <sub>2</sub> O <sub>3</sub> Monoxide <sup>b</sup> Spinel (8.10) <sup>b</sup> Spinel (8.35) CoWO <sub>4</sub>	Cr <sub>2</sub> O <sub>3</sub> Monoxide Spinel CoWO <sub>4</sub>
Hastelloy X					MAR M-200				
1800	982	ND	ND	Cr <sub>2</sub> O <sub>3</sub> Monoxide <sup>b</sup> Spinel (8.30)	1800	982	ND	ND	Cr <sub>2</sub> O <sub>3</sub> <sup>b</sup> Spinel (8.15)
1900	1038	ND	ND	Cr <sub>2</sub> O <sub>3</sub> <sup>b</sup> Spinel (8.25)	1900	1038	ND	ND	Cr <sub>2</sub> O <sub>3</sub> <sup>b</sup> Spinel (8.15)
2000	1093	ND	ND	Cr <sub>2</sub> O <sub>3</sub> <sup>b</sup> Spinel (8.25)	2000	1093	ND	ND	Monoxide <sup>b</sup> Spinel (8.15)

<sup>a</sup>Not determined.

<sup>b</sup>Values in parentheses are lattice parameters in angstroms (or  $\times 10^{-10}$  m).

<sup>c</sup>Tri-rutile structure; possibly nickel tantalate (NiTa<sub>2</sub>O<sub>5</sub>).

L-605 had the simplest oxides of the cobalt-base alloys examined. After 100 hours at 1800° and 1900° F (982° and 1038° C), only a monoxide and a spinel were observed. The cast cobalt-base alloys had some of the most complex oxides. They contained chromia, the monoxide, spinels, and cobalt tungstate. Chromia and the tungstate were missing from the X-40 scales at the highest temperature 2000° F (1093° C) and the longest time, 100 hours. On X-40 the tungstate was not observed after 1800° F (982° C) exposure or after test at 1900° and 2000° F (1038° and 1093° C) on any of the 20 hour specimens. Mar M-509A had only chromia at 1800° F (982° C) after 20 hours.

### Effect of Burner Conditions on Weight Loss and Cracking at 2000° F (1093° C)

Although most of the tests were run at the standard cycle of 1 hour at temperature in a Mach 1 gas stream followed by forced air cooling to room temperature, other modes of heating and cooling were also investigated. Three nickel-base and three cobalt-base alloys were tested at 2000° F (1093° C) using modified cycles.

Weight loss. - The weight loss results are listed in table V. The high gas velocity used in the standard cycle was one of the chief differences between the tests reported here and the more conventional static oxidation tests. In order to observe the effect of velocity, the combustion air was reduced as much as possible without damaging the burner. The three alloys, TD-NiCr, IN-100, and WI-52 were tested with a cycle equivalent to the standard cycle except for gas velocity. The burner exit velocity was reduced from Mach 1 to Mach 0.7.

The weight loss of TD-NiCr dropped to only 0.60 of the standard weight loss. This may have been due to a decreased evaporation rate of chromia at the reduced gas velocity. Although chromia was found on static oxidation specimens of TD-NiCr, none was found on the specimens exposed to oxidation in the burner facility.

The IN-100 specimens showed a 60 percent increase in weight loss over the standard weight loss. This increase in weight loss has not been explained.

In addition to the high velocity gas stream, the other feature of the test conditions believed to accelerate weight loss was cyclic operation which induced spalling by means of thermal stresses. An approach to steady-state operation was made by using cycles approximately 10 hours long. The specimens were allowed to cool freely in air rather than in the Mach 1 air jet of the standard test. The materials tested were TD-NiCr, IN-100, WI-52, B-1900, X-40, and Mar M-509A. In this test all these materials lost appreciably less weight than in the standard test. The least benefitted were TD-NiCr, which lost 0.78 of the amount lost during the standard cycle, and X-40, which lost 0.75 of the standard test loss. Mar M-509A was most benefitted, losing only 0.16 of that lost in

TABLE V. - EFFECT OF OPERATING CONDITIONS ON WEIGHT LOSS

Maximum cycle temperature,  $T_{max}$ , 2000° F (1093° C).

Alloy	Weight loss after 100 hours at 2000° F, mg			
	Standard cycle	Other modes of operation (a)		
		Mach 1, forced-air cool, $T_{max}$ to room temperature, 1-hr cycles	Mach 0.7, forced-air cool, $T_{max}$ to room temperature, 1-hr cycles	Mach 1, free-air cool, $T_{max}$ to room temperature, ~10-hr cycles
IN-100	250	395 (1.58)	158 (0.63)	169 (0.68)
TD-NiCr	1 400	841 (0.60)	1091 (0.78)	-----
WI-52	23 700	22 116 (0.93)	9852 (0.42)	9840 (0.41)
B-1900	216	-----	127 (0.59)	145 (0.67)
X-40	1 240	-----	914 (0.74)	-----
MAR M-509A	4 870	-----	795 (0.16)	-----

<sup>a</sup>Values inside parentheses are ratio of weight loss in other mode of operation to weight loss in standard cycle.

the standard test; next was WI-52 which lost 0.42 of the standard amount. It has been suggested by C. Lowell of this laboratory that WI-52 has a strong tendency to spall on cooling because of the volume contraction which results when the cobalt oxide, CoO, stable at high temperature, changes to the spinel, Co<sub>3</sub>O<sub>4</sub>, stable at lower temperatures. Fewer and less severe thermal cycles should reduce the opportunity for this reaction to cause spalling. Although this explanation is plausible for WI-52 and Mar M-509A, it does not account for X-40, which was much less benefitted by the reduced severity of thermal cycling yet developed essentially the same oxides (see table IV) as the other two cobalt-base alloys. On the other hand, the X-40 scale was thinner than the scale of the other two alloys and would not be expected to spall as much so that there was less room for improvement.

A third mode of cooling was used in a test of IN-100, WI-52, and B-1900. Instead of cooling to room temperature between heating cycles, the specimens were held in the cooling air blast only long enough to cool a thermocouple embedded in a dummy specimen to 1200° F (649° C). The specimens were then returned to the hot gas stream and the test continued. The relative reductions in weight lost were almost the same for this

test as in the test simulating steady-state operation. This suggests that each cycle of rapid cooling to 1200° F (649° C) caused even less spalling than a cycle of slow cooling to room temperature. It must be remembered that there were 100 cycles of cooling rapidly to 1200° F (649° C) and only 10 cycles of slow cooling to room temperature.

Thermal fatigue. - The effects of the modified cycles on thermal fatigue are shown in figure 20. The heating conditions at Mach 0.7 and at Mach 1.0, were not enough different to cause any observable difference in the cracking of IN-100. No cracks occurred in WI-52 at Mach 0.7, whereas cracks had appeared as early as 40 hours at Mach 1.0.

The simulated steady state caused no cracking for any of the alloys, representing a substantial improvement for WI-52, IN-100, and B-1900. Although the difference between weight losses under the "steady-state" conditions and the cycle between 2000° and 1200° F (1093° and 649° C) were very slight, the difference in cracking behavior between these two modified cycles was marked. The cracking of B-1900 and IN-100 was nearly as severe for the 2000° to 1200° F (1093° to 649° C) cycle as it was under standard conditions. No cracking was observed for WI-52 when cycled over the narrower temperature range.

## SUMMARY OF RESULTS

An investigation was conducted to determine the resistance to oxidation of typical gas turbine alloys exposed alternately to high and low temperature, high velocity, gas streams. A natural gas-compressed air burner was used to produce velocities up to Mach 1 and specimen temperatures up to 2000° F (1093° C). The materials tested included six nickel-base alloys: IN-100, B-1900, Mar M-200, TAZ-8A, Hastelloy X, and TD-NiCr, and four cobalt alloys: L-605, X-40, Mar M-509A, and WI-52. The following results were obtained:

1. In a standard test used for all alloys, consisting of 100 cycles of 1 hour at temperature in a Mach 1 gas stream followed by rapid cooling to room temperature, the nickel-base alloys as a class experienced less weight loss than the cobalt-base alloys. Of the cobalt-base alloys, X-40 had the lowest weight loss which was only slightly less than Mar M-200. The latter alloy had the highest weight loss of all the nickel-base alloys tested. The cast cobalt-base alloy, WI-52, was the least oxidation resistant alloy tested. The materials varied widely in their resistance to oxidation. The average value of weight loss for each alloy after 100 hours at 2000° F (1093° C) was as follows: B-1900, 216 mg; IN-100, 250 mg; TAZ-8A, 305 mg; TD-NiCr, 1400 mg; Hastelloy X, 1450 mg; Mar M-200, 1500 mg; X-40, 1240 mg; Mar M-509A, 4870 mg; and WI-52, 23 700 mg.

2. After 100 hours surface recession paralleled weight loss. For the materials tested for surface recession, the values after 100 hours at 2000<sup>o</sup> F (1093<sup>o</sup> C) were as follows: B-1900, 0.3 mils; IN-100, 0.3 mils; TD-NiCr, 2.4 mils; X-40, 1.6 mils; Mar M-509A, 14 mils; and WI-52, 50 mils.

3. Comparison of weight loss measurements of alloys tested under cyclic conditions in a high velocity gas stream with weight gain data obtained in static oxidation tests indicated the following:

a. Differences between materials were greater in the high velocity tests.

b. Ranking of materials was quite different in the two types of tests.

4. As a class, conventionally cast cobalt-base alloys were more resistant to thermal fatigue cracking than conventionally cast nickel-base alloys. However, the wrought nickel-base alloy, Hastelloy X, and the dispersion strengthened TD-NiCr were among the most crack resistant alloys tested. For example, after 40 standard cycles with the maximum temperature at 2000<sup>o</sup> F (1093<sup>o</sup> C), all the IN-100, B-1900, and equiaxed Mar M-200 specimens and over half the TAZ-8A specimens were cracked. Under the same conditions, none of the X-40 or Mar M-509 specimens and less than half the WI-52 specimens were cracked. TD-NiCr at 2000<sup>o</sup> F (1093<sup>o</sup> C) developed no cracks until after 80 cycles and Hastelloy X had no cracks even after 100 cycles at 2000<sup>o</sup> F (1093<sup>o</sup> C). All the L-605 specimens tested at 1800<sup>o</sup> and 1900<sup>o</sup> F (982<sup>o</sup> and 1038<sup>o</sup> C) cracked before 40 cycles.

5. Directionally solidified and single grain castings of Mar M-200 exhibited no cracks even after 100 cycles at 2000<sup>o</sup> F (1093<sup>o</sup> C), while the equiaxed castings cracked in 20 cycles or less. However, castings having the controlled macrostructures showed between two and five times as much weight loss as conventionally cast (equiaxed) castings.

6. Limited testing with modified cycles at 2000<sup>o</sup> F (1093<sup>o</sup> C) showed the following:

a. Under simulated steady-state operation (10-hour cycles with free air cool to room temperature) the weight loss for the six alloys tested was less than that obtained under standard cyclic conditions. The reduction in weight loss observed was in the proportions shown: TD-NiCr, 0.78; X-40, 0.74; IN-100, 0.63; B-1900, 0.59; WI-52, 0.42; and Mar M-509A, 0.16.

No cracking was observed in any of these alloys under these conditions.

b. In a test where the lower temperature during a cycle was restricted to 1200<sup>o</sup> F (649<sup>o</sup> C) rather than room temperature as in the standard cycle, the weight loss dropped from the loss observed in the standard test cycle in the proportions shown: IN-100, 0.68; WI-52, 0.41; B-1900, 0.67.

The propensity toward cracking appeared to be unchanged for IN-100 and B-1900, but was substantially reduced for WI-52.

Lewis Research Center,  
National Aeronautics and Space Administration,  
Cleveland, Ohio, April 15, 1969,  
720-03-02-37-22.

## REFERENCES

1. Donachie, M. J.; Sprague, R. A.; Talboom, F. P.; and Bradley, E. F.: Effects of Turbine Atmospheres on Sulfidation Corrosion. Paper 67-GT-2, ASME, Mar. 1967.
2. Sippel, George R.; Kildsig, John R.: Laboratory Tests for Evaluation of Surface Deterioration in Gas Turbine Engine Materials. Allison Res. Eng., vol. 10, 1966, pp. 20-35.
3. Nichols, E. S.; Burger, J. A.; and Hanink, D. K.: Comparative Evaluation of Protective Coatings for High Temperature Alloys. Paper 843E, SAE, Apr. 1964.
4. Bergman, P. A.; Sims, C. L.; and Beltran, A. N.: Development of Hot-Corrosion-Resistant Alloys for Marine Gas Turbine Service. Hot Corrosion Problems Associated with Gas Turbines. Spec. Tech. Publ. No. 421, ASTM, 1967, pp. 38-63.
5. Schirmer, R. M.; and Quigg, H. T.: Effect of Sulfur in JP-5 Fuel on Hot Corrosion of Coated Superalloys in Marine Environment. Proceedings of the Eighth Annual National Conference on Environmental Effects on Aircraft and Propulsion Systems. Institute of Environmental Sciences, 1968, pp. 143-159.
6. Waters, William J.; and Freche, John C.: Investigation of Columbium-Modified NASA TAZ-8 Superalloy. NASA TN D-3597, 1966.
7. Pearcey, B. J.; Kear, B. H.; and Smashey, R. W.: Correlation of Structure with Properties in a Directionally Solidified Nickel-Base Superalloy. Trans. ASM, vol. 60, no. 4, Dec. 1967, pp. 634-645.
8. Wolf, James S.; and Sandrock, Gary D.: Some Observations Concerning the Oxidation of the Cobalt-Base Superalloy L-605 (HS-25). NASA TN D-4715, 1968.
9. Lund, Carl H.; and Wagner, Herbert J.: Oxidation of Nickel- and Cobalt-Base Superalloys. DMIC Report 214, Battelle Memorial Inst. Mar. 1, 1965.

10. Anon.: Interim Data Sheet, Dupont Metal Products - New Products Information. Dupont Metals Center, Baltimore, Md., Aug. 1966.
11. Wheaton, H. L.: Mar-M 509, A New Cast Cobalt-Base Alloy for High-Temperature Service. Cobalt, no. 29, Dec. 1965, pp. 163-170.

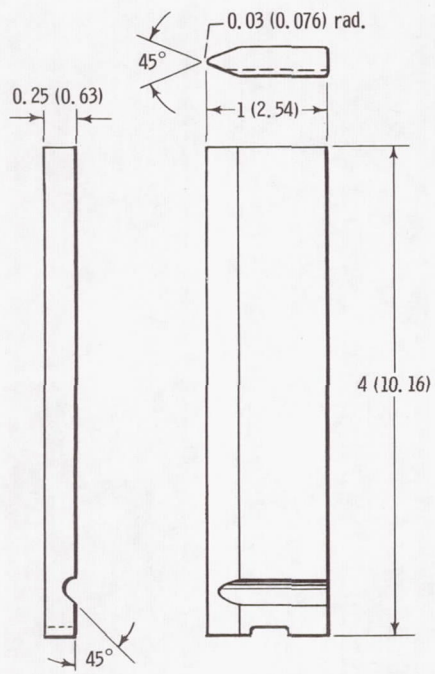
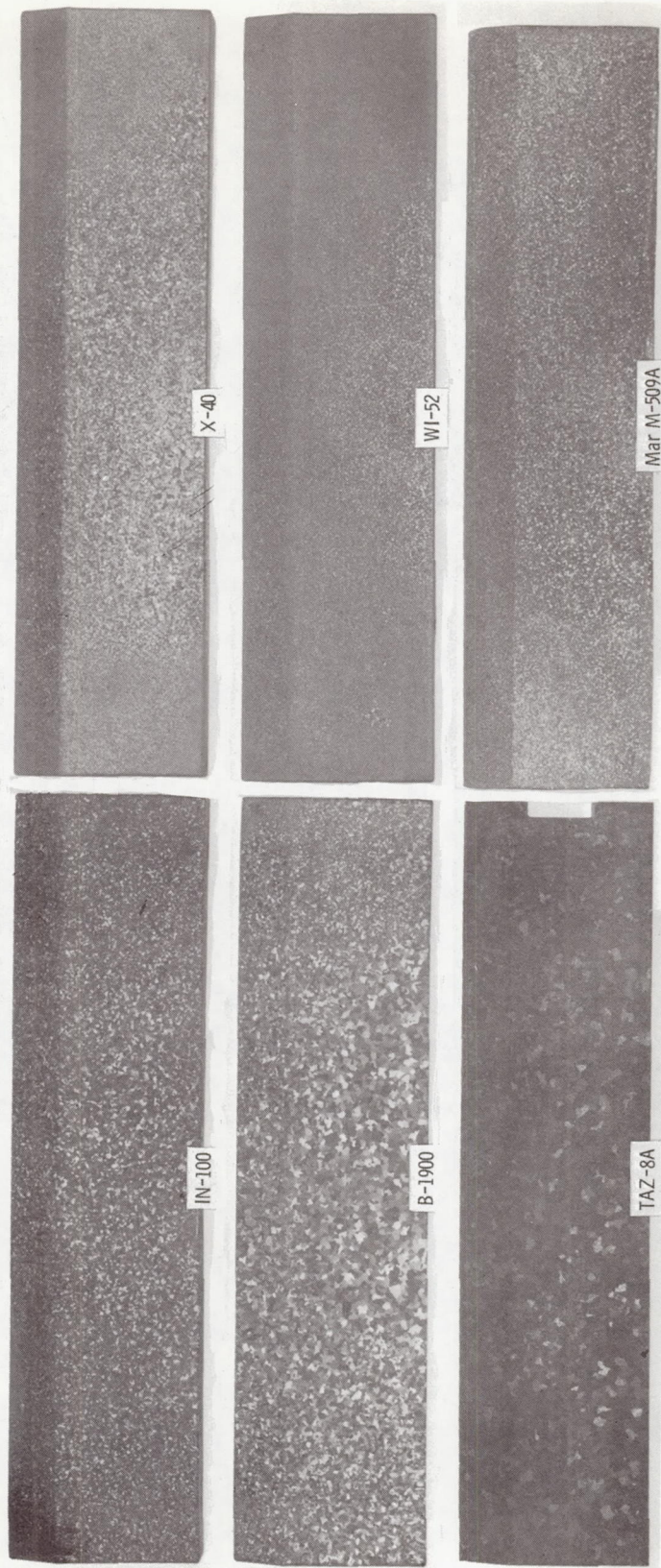
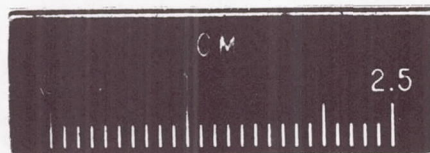
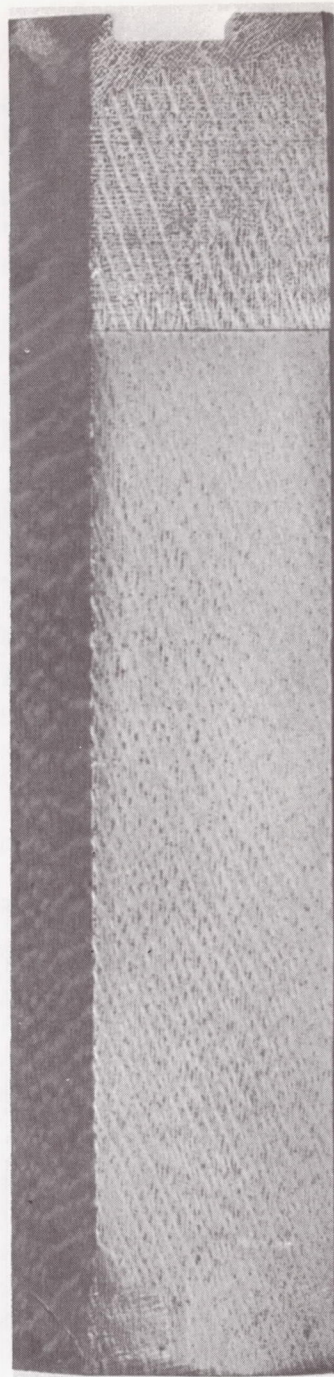


Figure 1. - High-velocity oxidation specimen.  
(Dimensions are in inches (cm).)



C-68-2276

Figure 2. - Macrostructure of investment cast specimens.



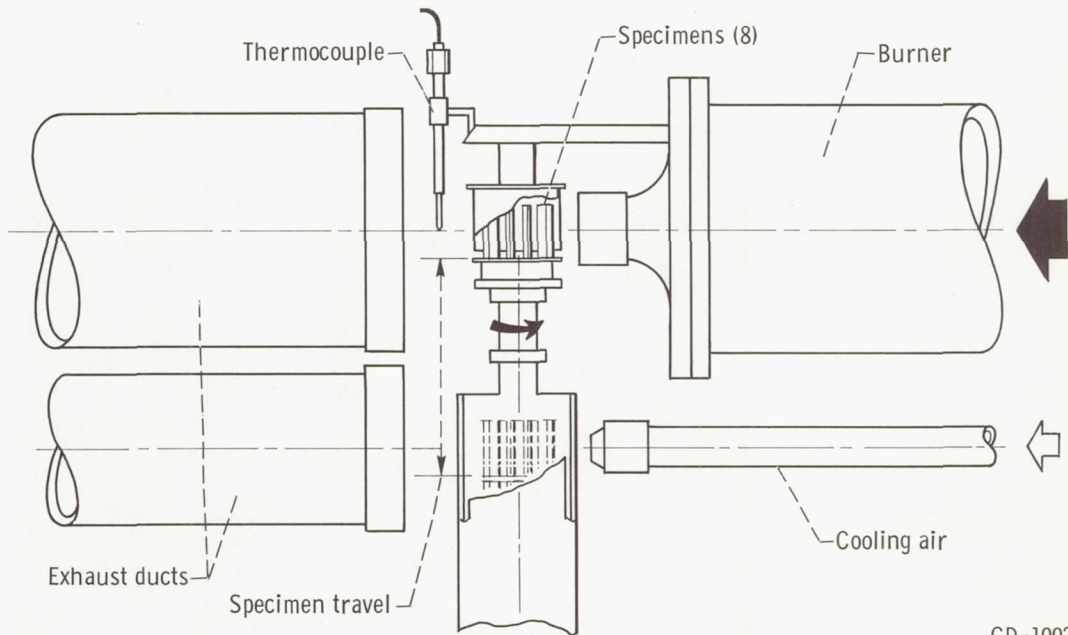
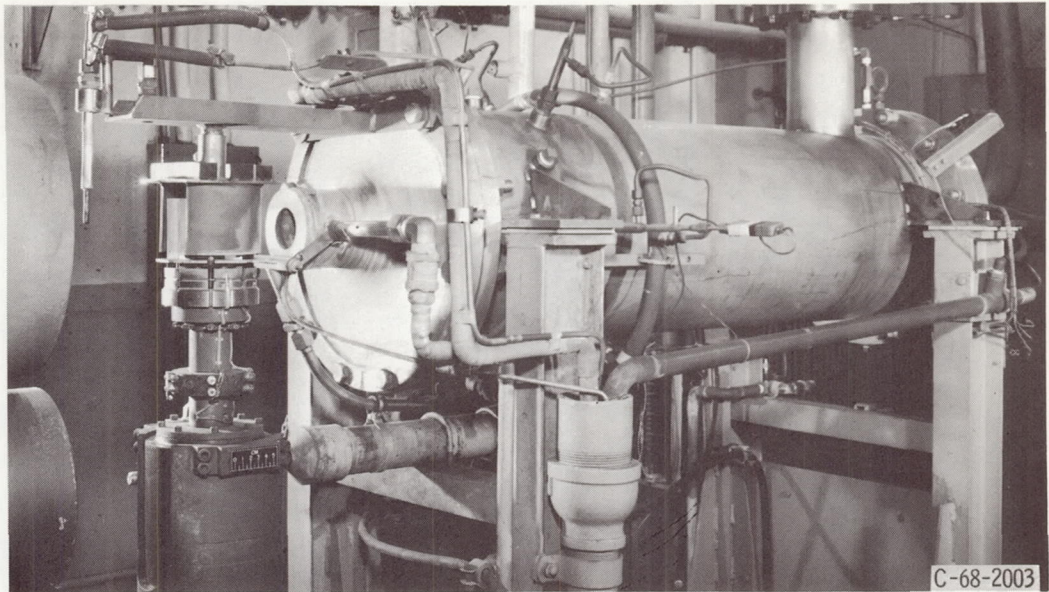
Conventionally cast

Directionally solidified

Single grain

C-68-2278

Figure 3. - Macrostructure of Mar M-200 specimens.



CD-10022-17

Figure 4. - High-gas-velocity oxidation apparatus.

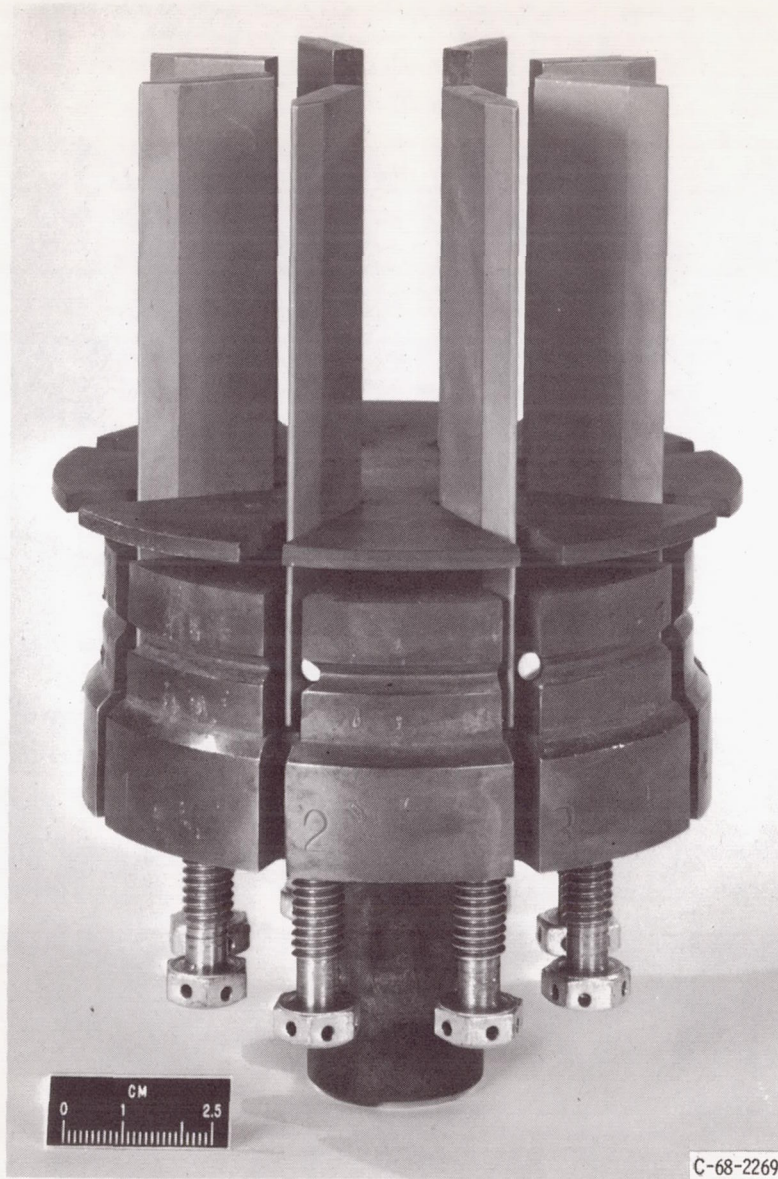


Figure 5. - Specimen holder assembly.

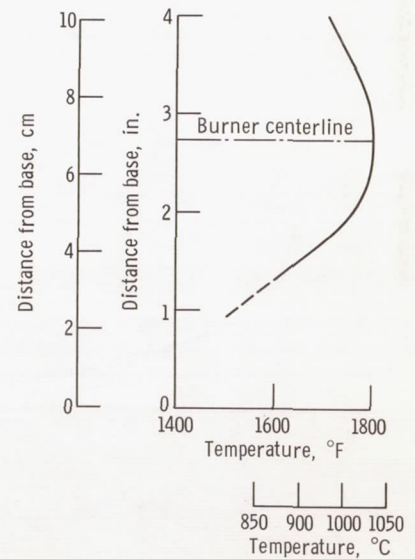
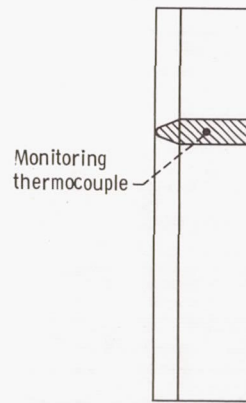
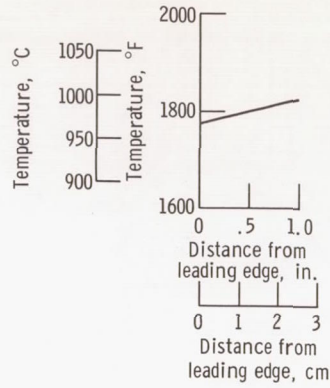
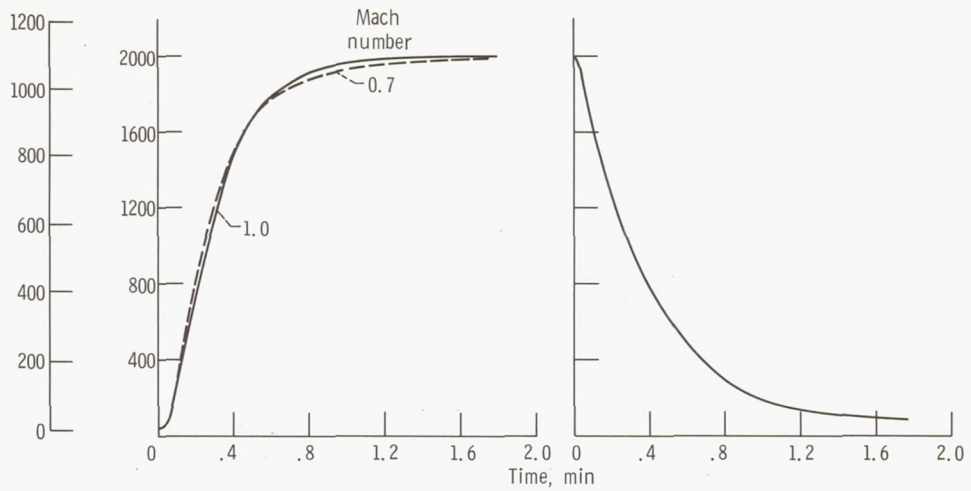
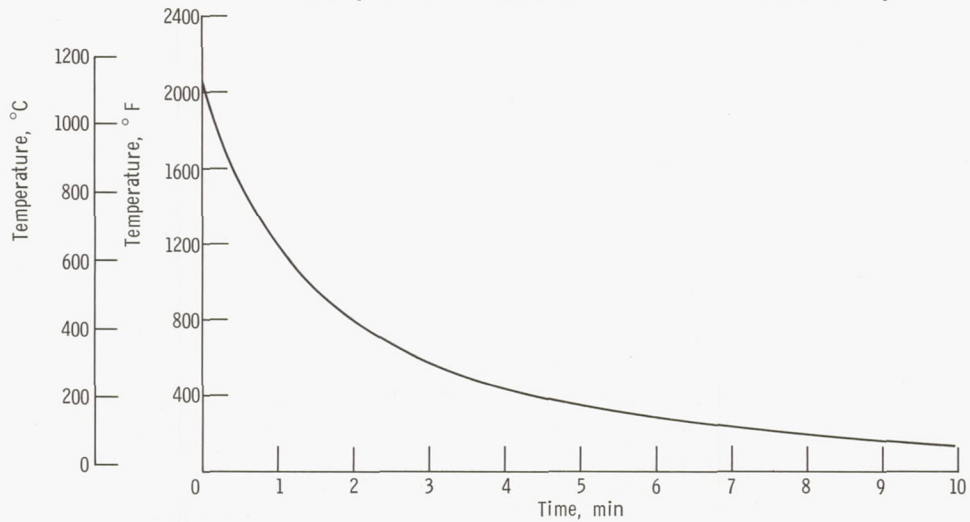


Figure 6. - Typical chordwise and axial temperature profiles of oxidation specimen during exposure at Mach 1 for test temperature of 1800° F (982° C).

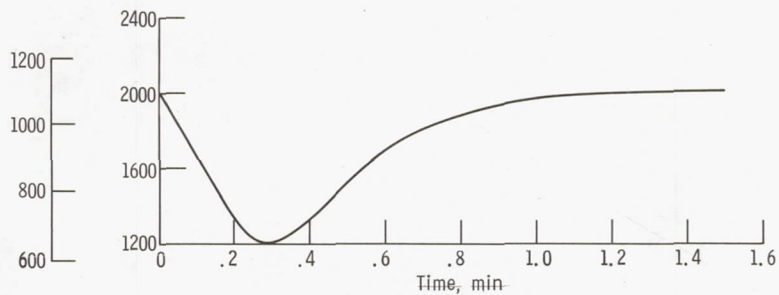


(a) Standard heating (Mach 1.0) and Mach 0.7.

(b) Standard cooling.



(c) Slow cooling (steady-state cycle).



(d) Short cooling cycle.

Figure 7. - Typical heating and cooling curves for oxidation specimens during various test cycles.

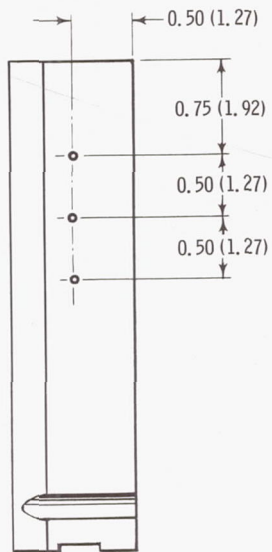


Figure 8. - Location of platinum pins  
in recession measurement specimens.  
(Dimensions in inches (cm).)

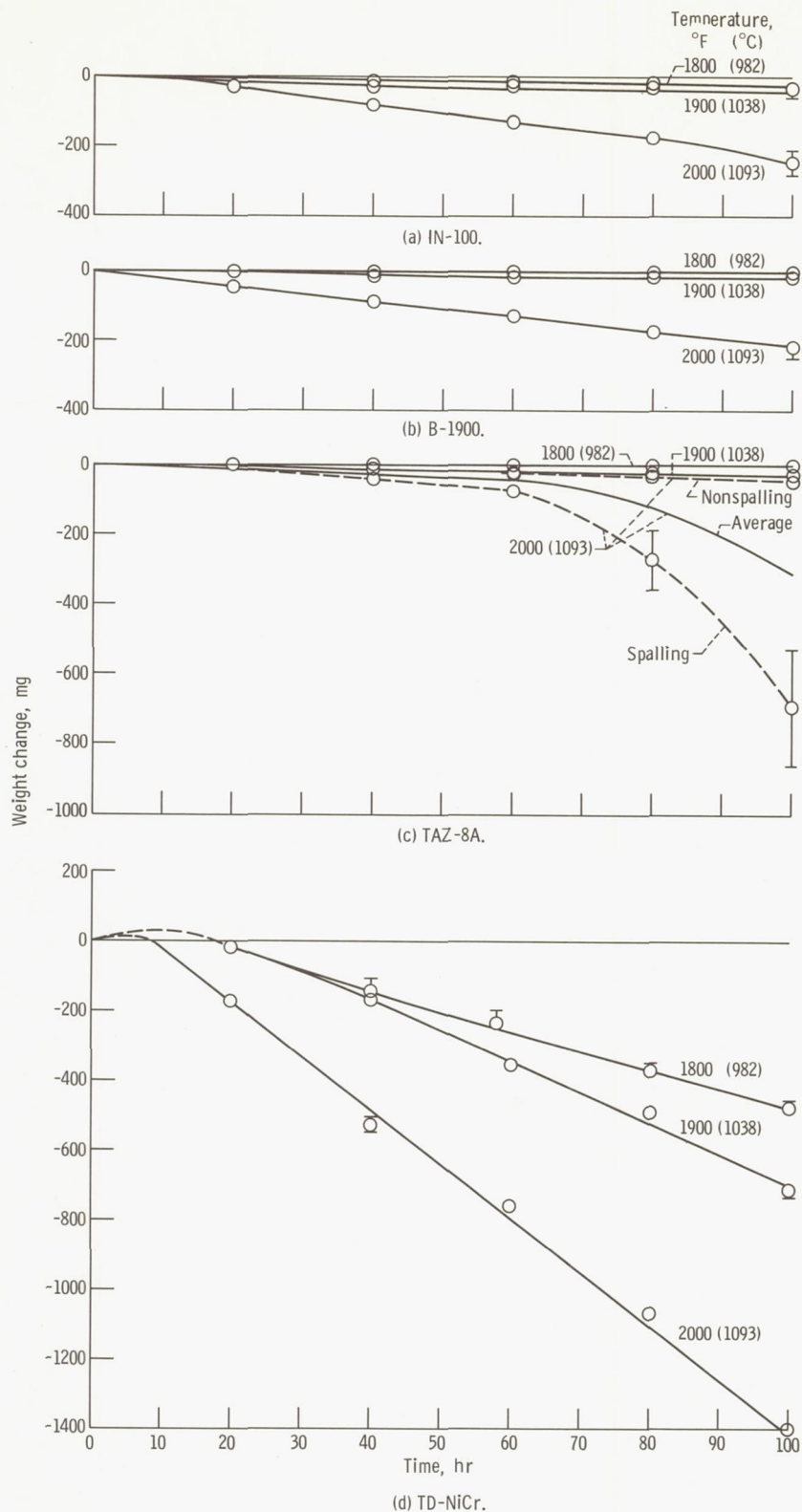


Figure 9. - Weight change of materials at various temperatures during exposure to high-gas-velocity oxidation apparatus. Test cycle: 1 hour at test temperature, 3 minutes at room temperature.

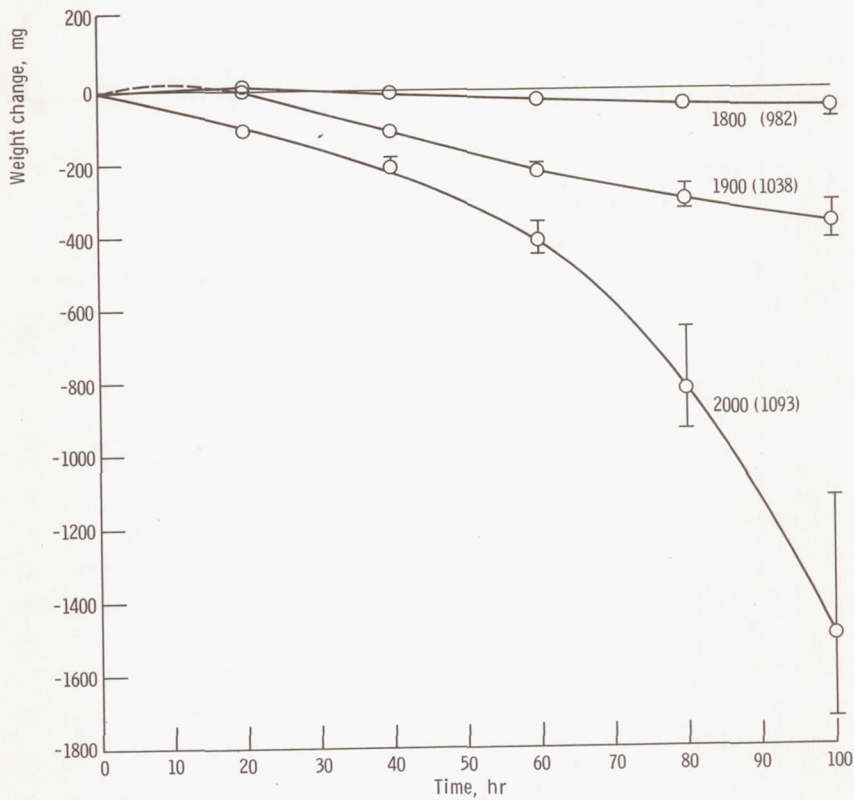
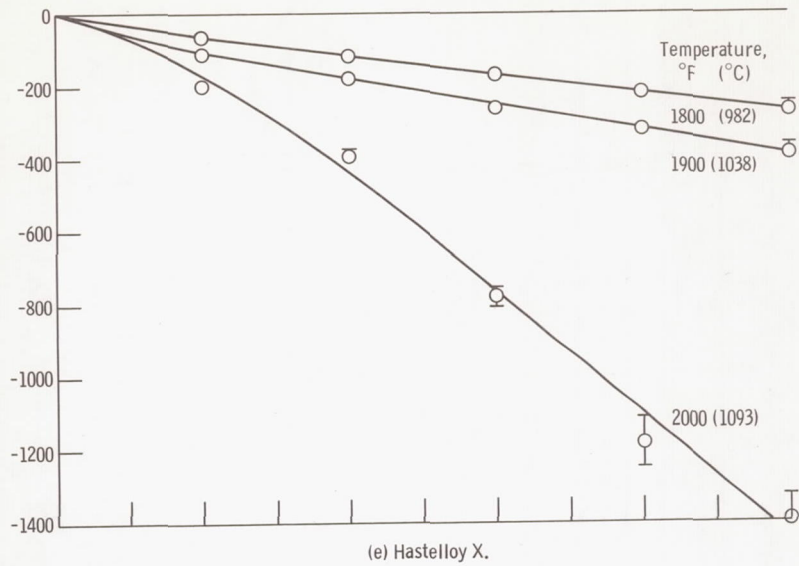


Figure 9. - Continued.

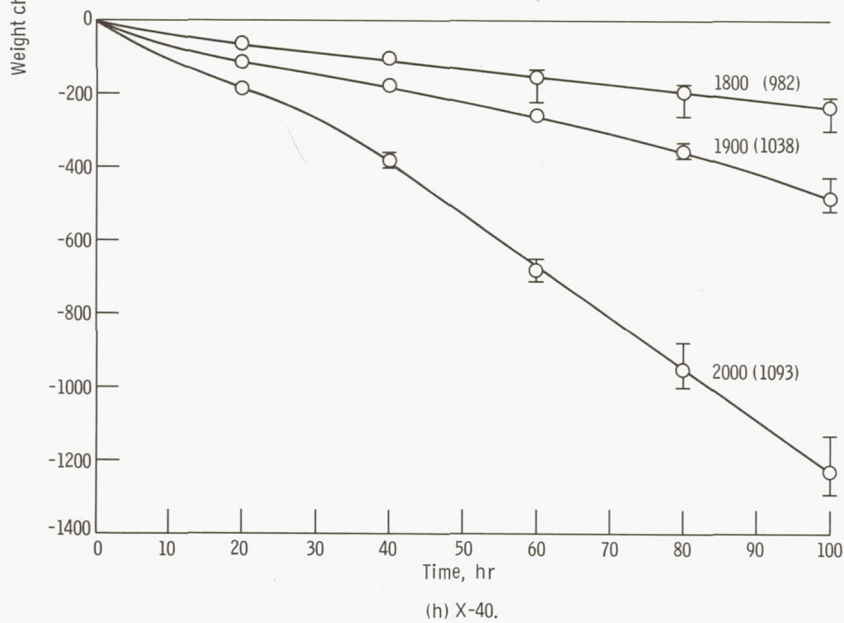
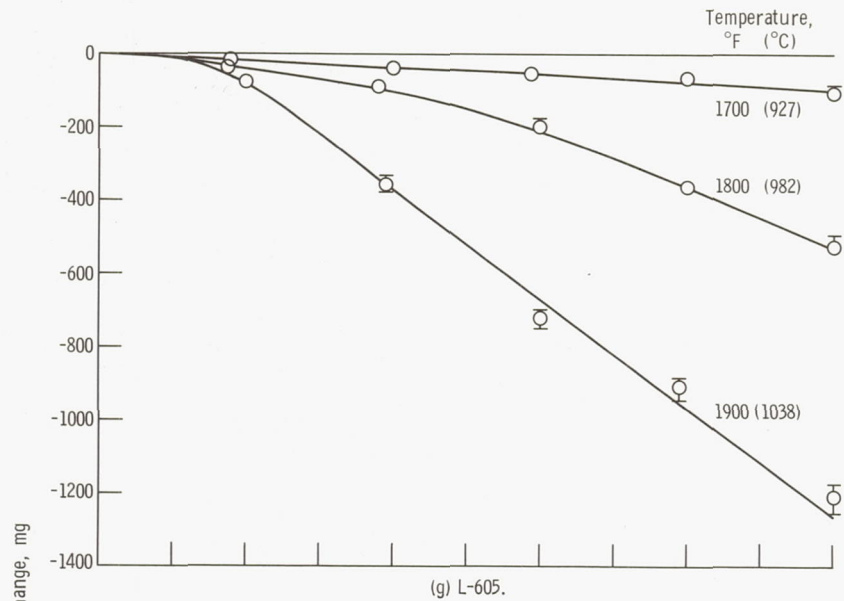
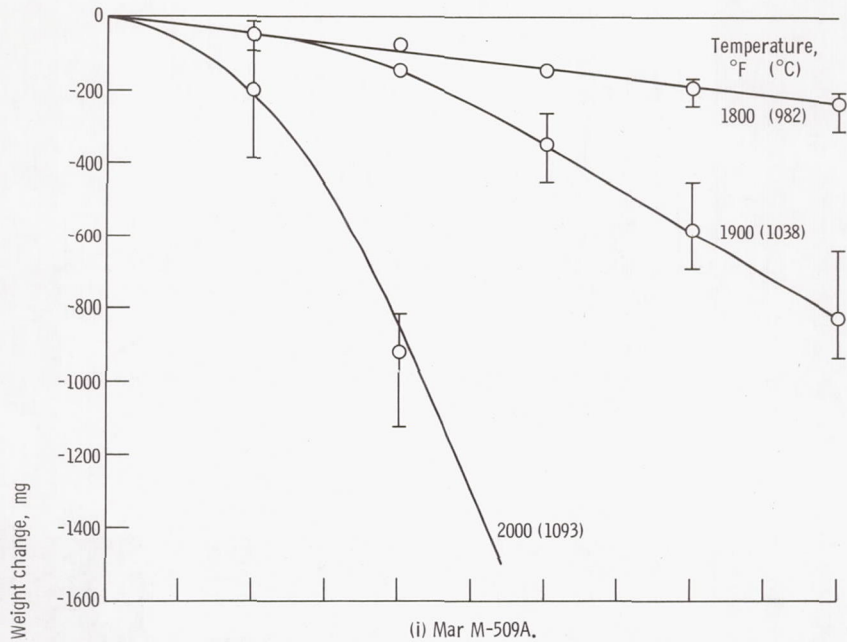
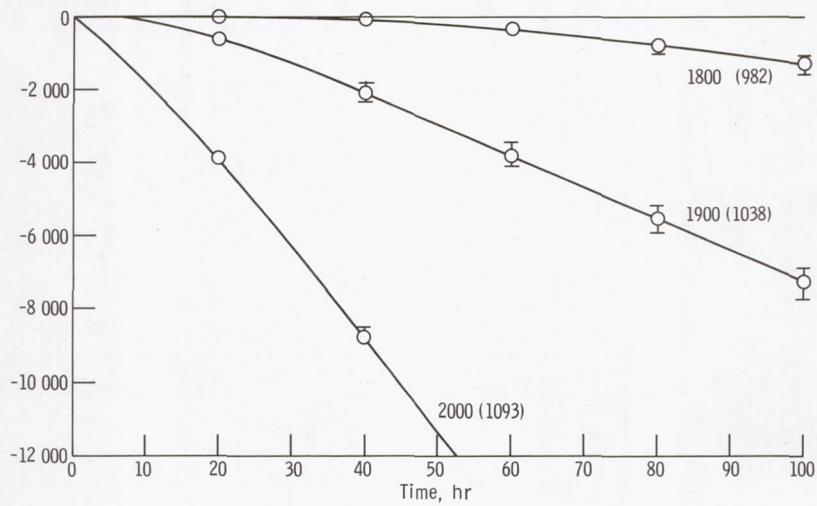


Figure 9. - Continued.



(i) Mar M-509A.



(j) WI-52.

Figure 9. - Concluded.

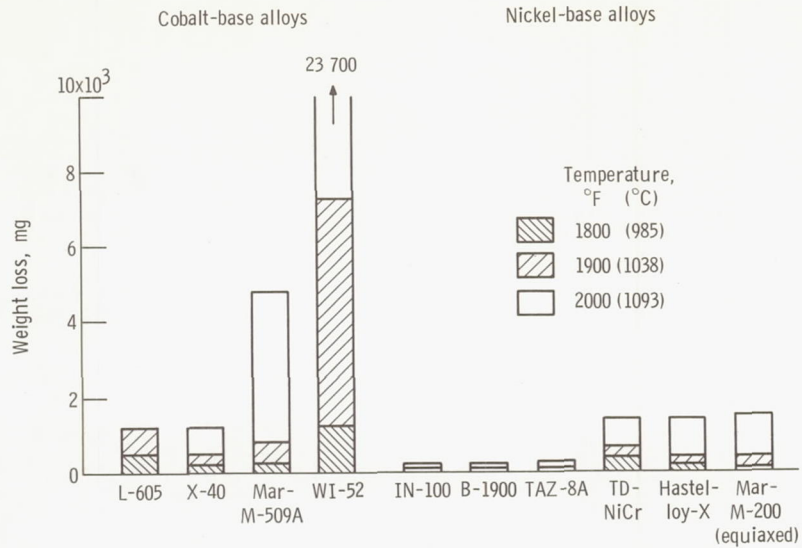


Figure 10. - Summary of weight loss data for materials exposed 100 hours to high-gas-velocity oxidation apparatus.

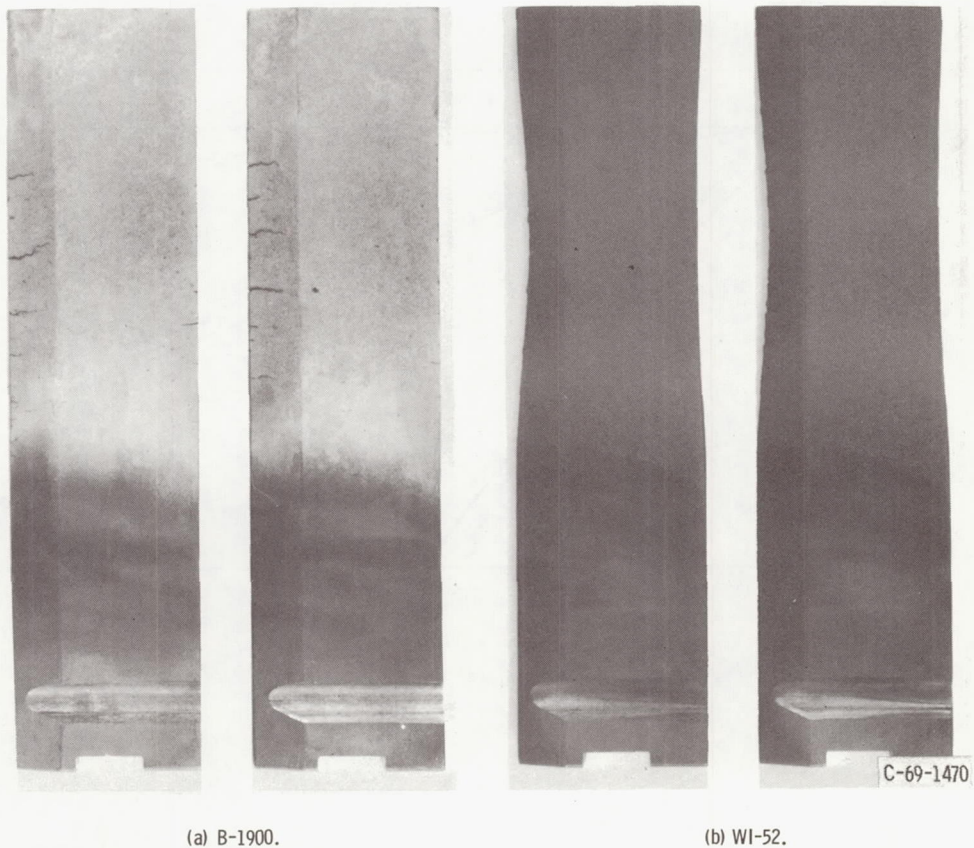


Figure 11. - Condition of oxidation specimens after exposure for 100 hours (cycles) at 2000° F (1093° C).

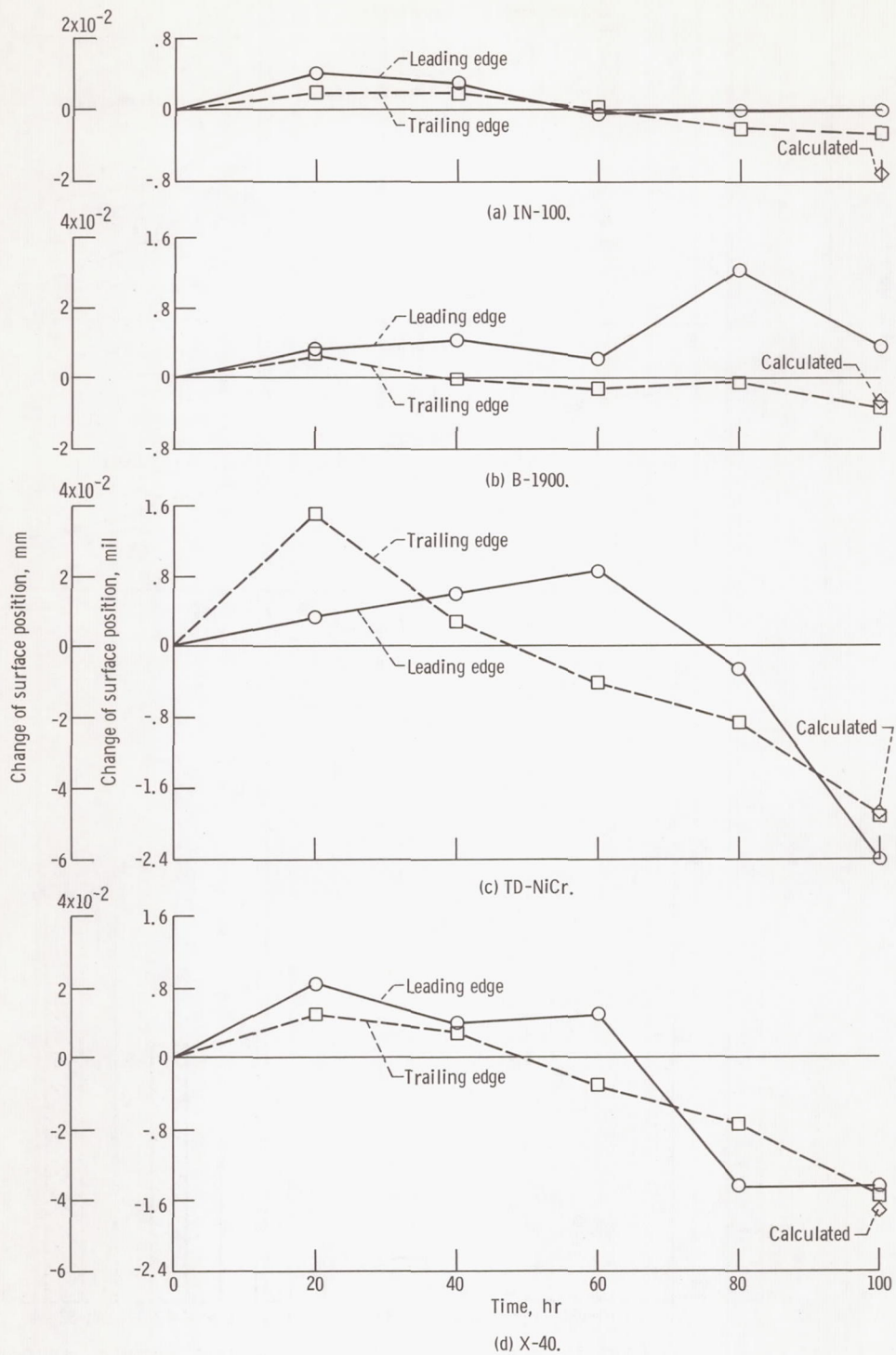


Figure 12. - Surface recession of oxidation specimens. Standard cycle; maximum temperature, 2000° F (1093° C).

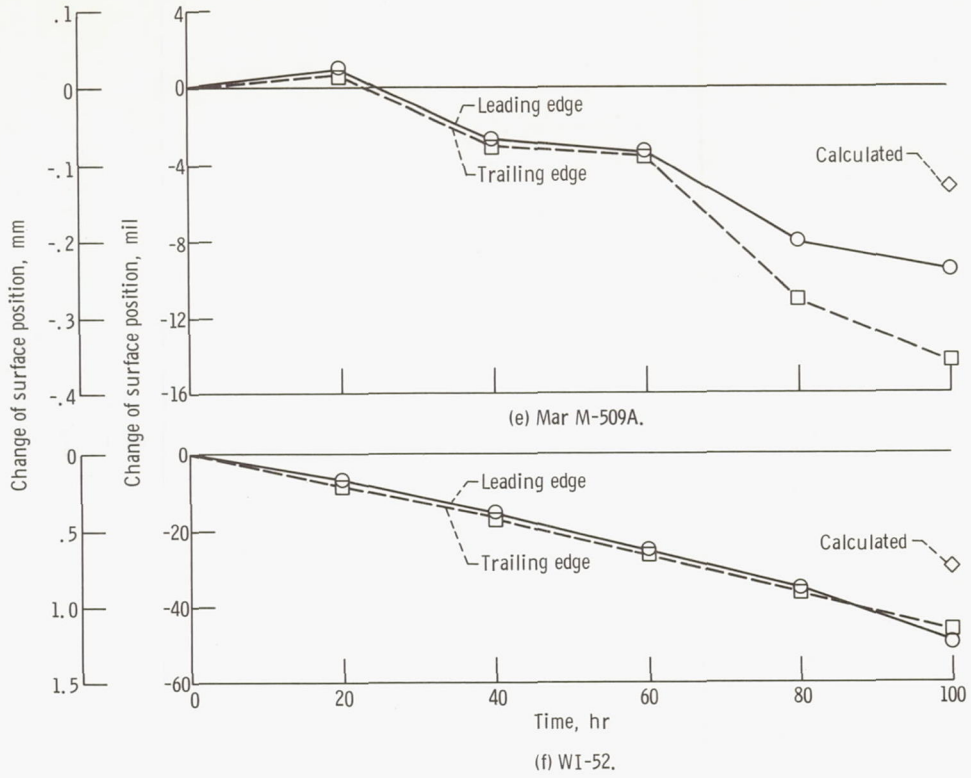


Figure 12. - Concluded.

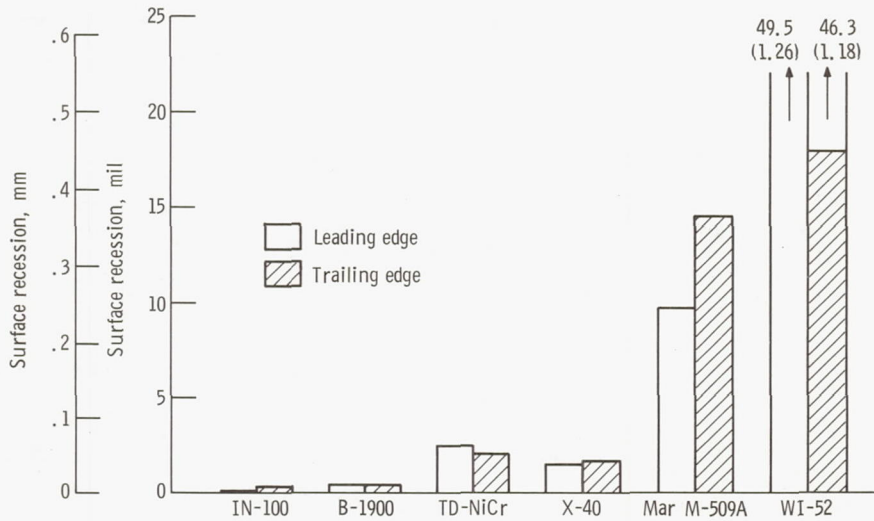
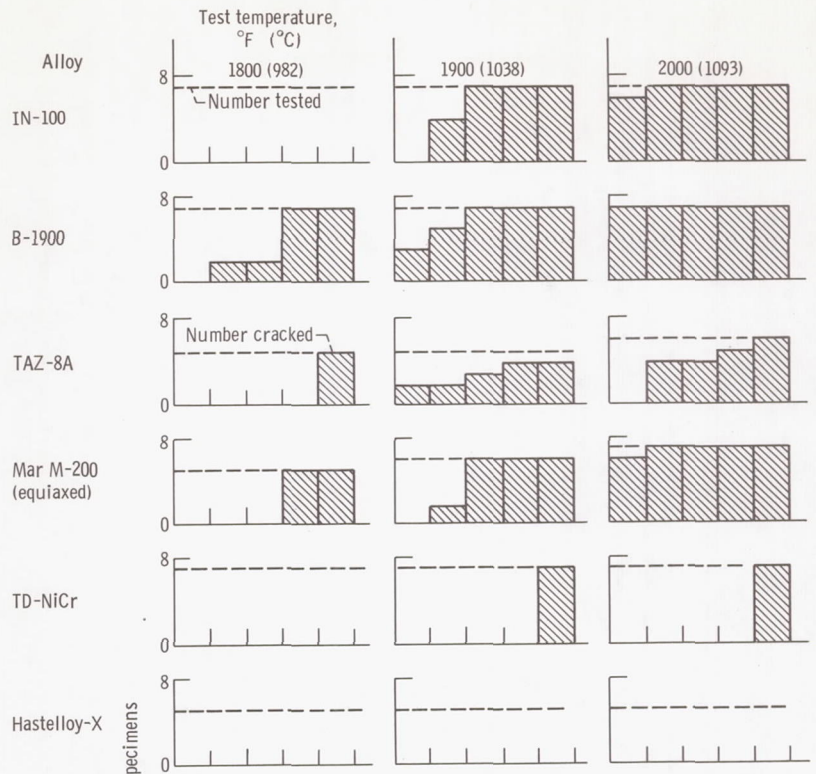
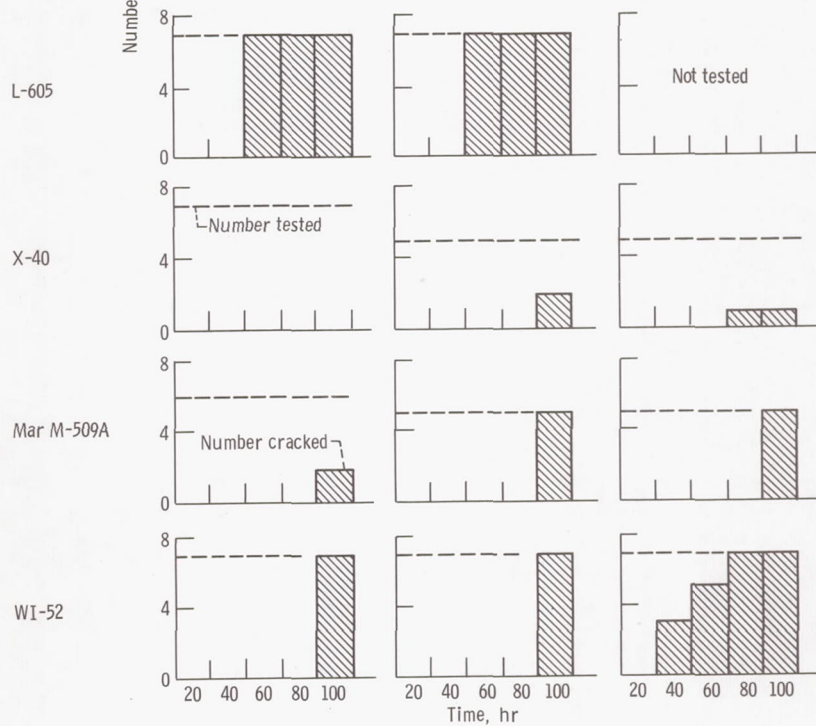


Figure 13. - Summary of surface recession measurements after 100 hours at 2000° F (1093° C) using standard cycle.

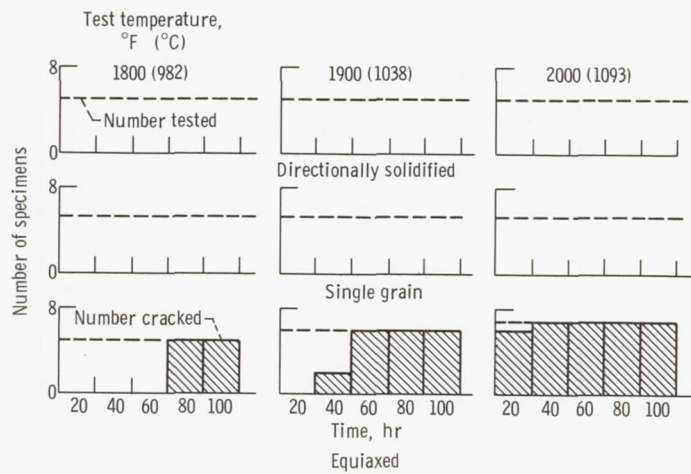


(a) Nickel-base alloys.



(b) Cobalt-base alloys. (L-605 not tested at 2000° F (1093° C).)

Figure 14. - Thermal fatigue cracking of materials at various temperatures during exposure to high-gas-velocity oxidation apparatus using standard cycle.



(c) Controlled solidification Mar M-200 alloy.

Figure 14. - Concluded.

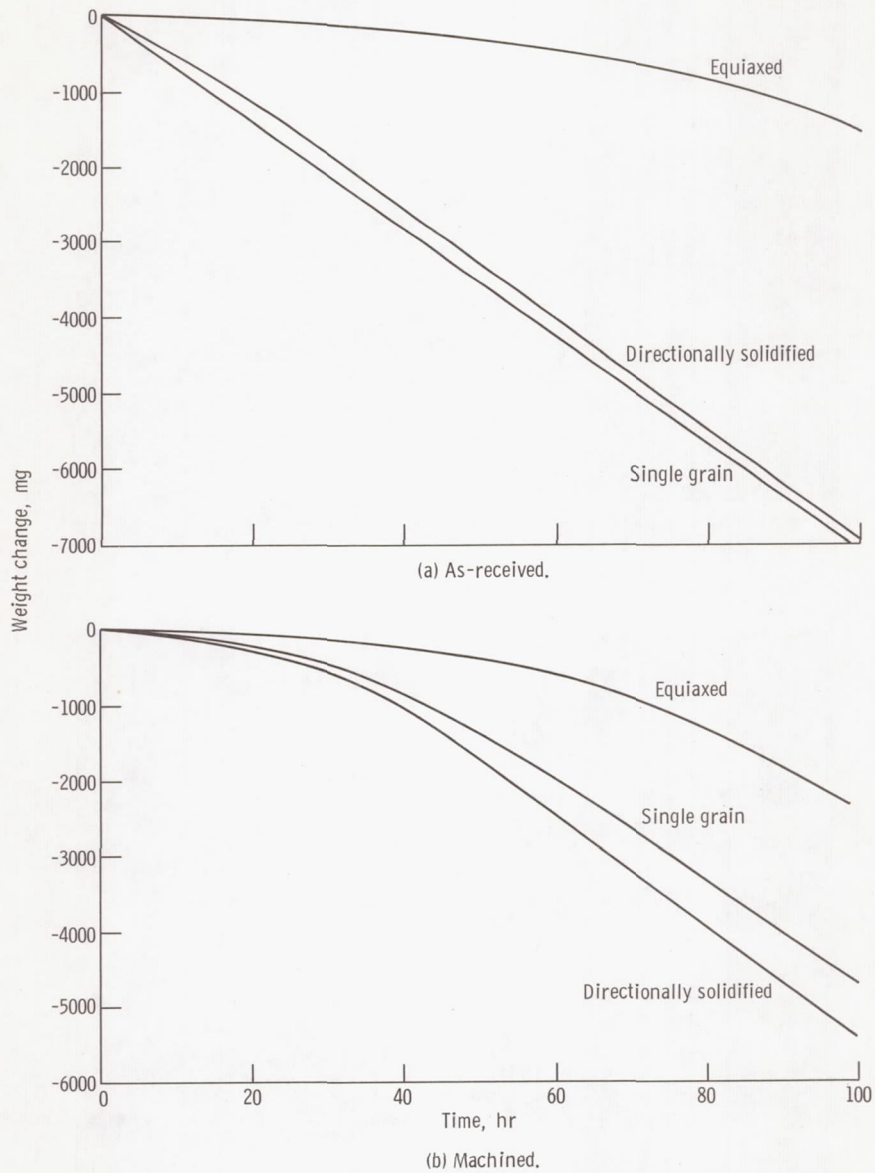
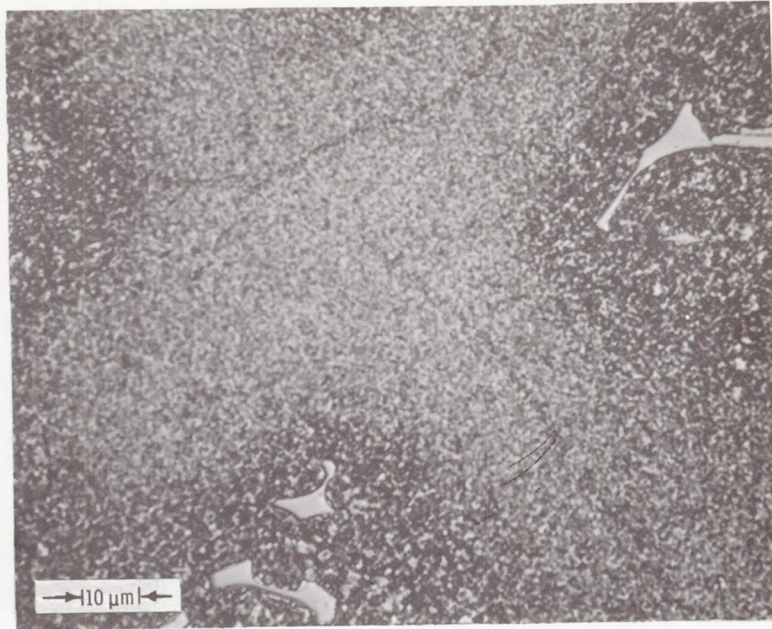
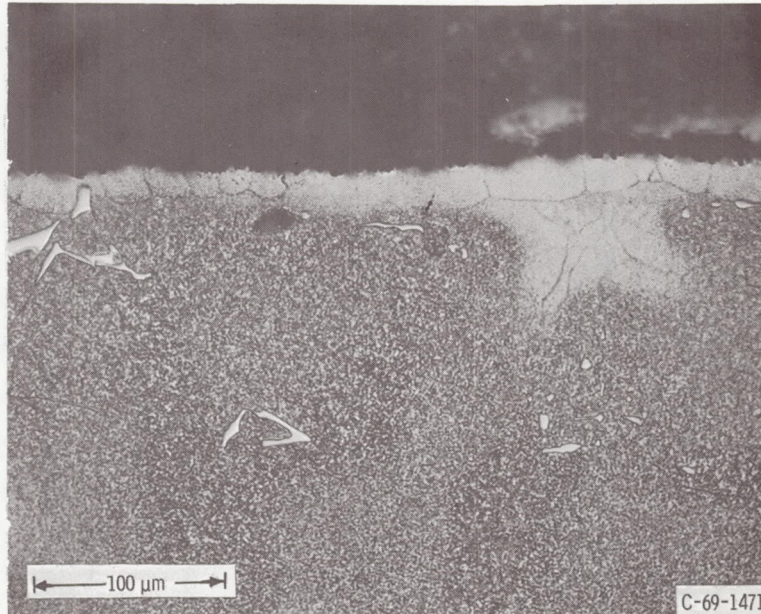


Figure 15. - Comparison of high-gas-velocity oxidation behavior of three macrostructures of Mar M-200 after exposure to standard cycle at 2000° F (1093° C) maximum temperature.

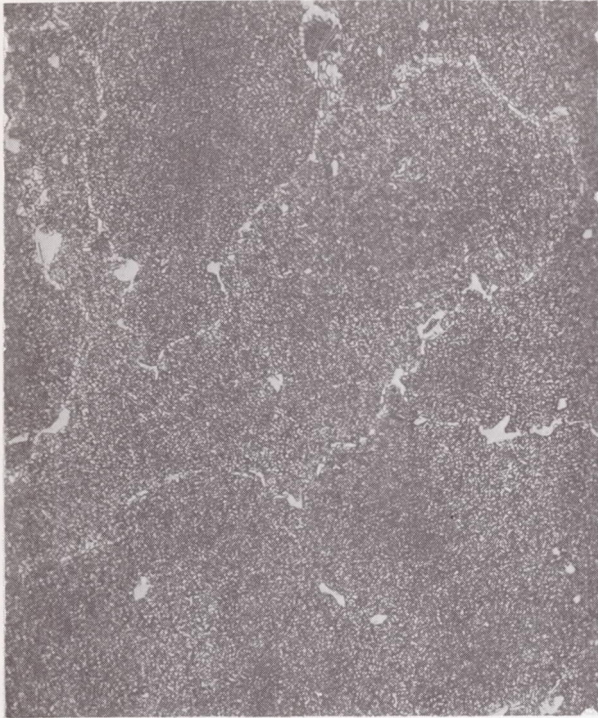


(a) Center; X750.



(b) Edge; X250.

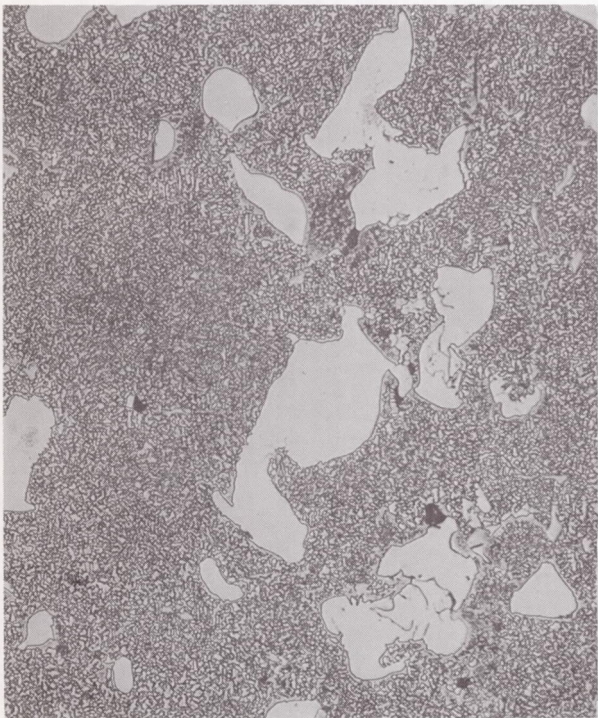
Figure 16. - Photomicrographs of as-received single crystal casting of Mar M-200.



(a) IN-100.



(b) B-1900.

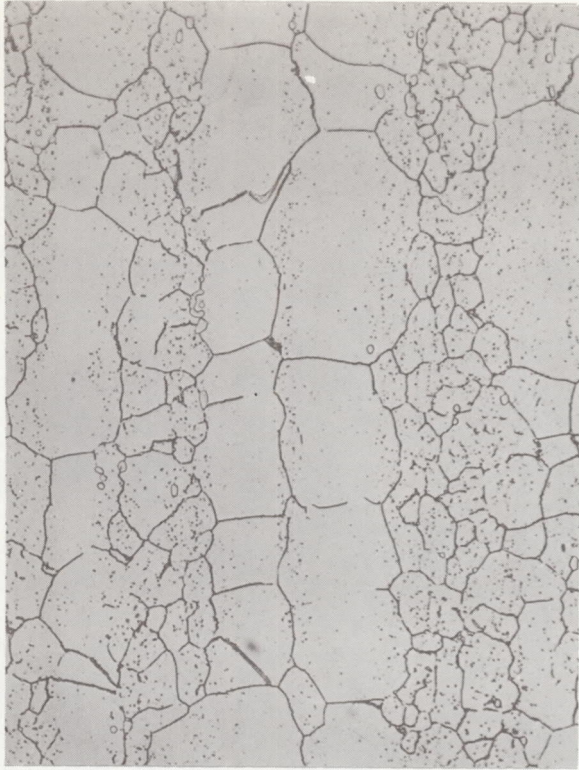


(c) TAZ-8A.

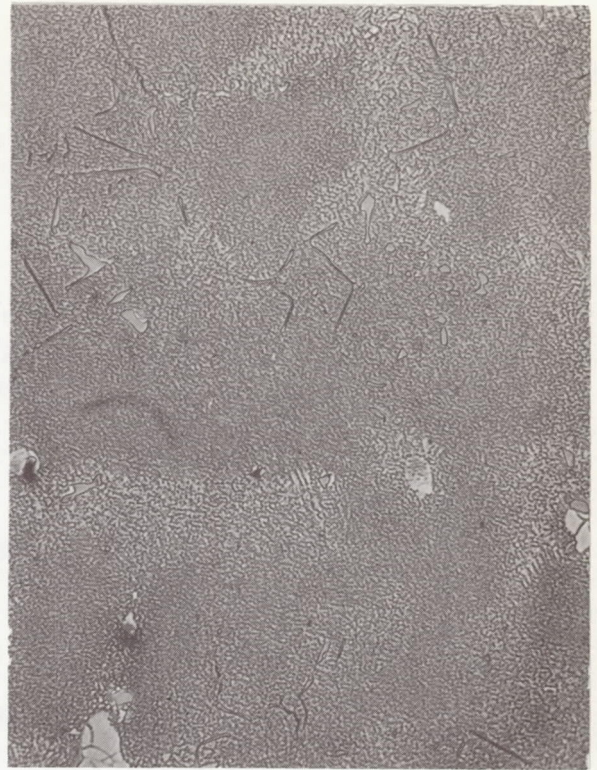


(d) TD-NiCr.

Figure 17. - Microstructures of as-received materials. X250.



(e) Hastelloy X.



(f) Mar M-200 (equiaxed).

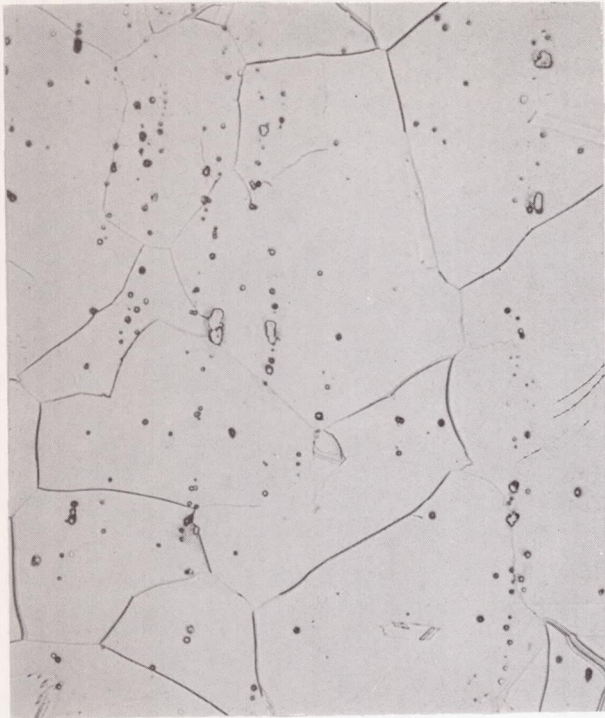


(g) Mar M-200 (directionally solidified).

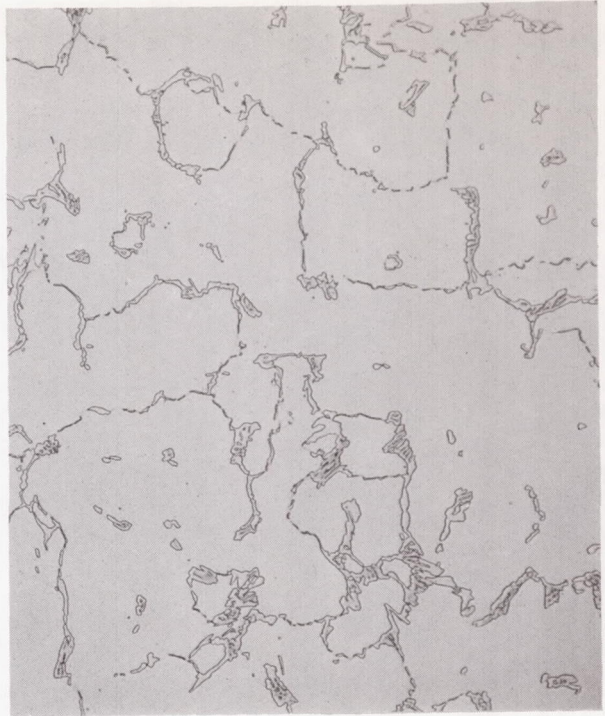


(h) Mar M-200 (single grain).

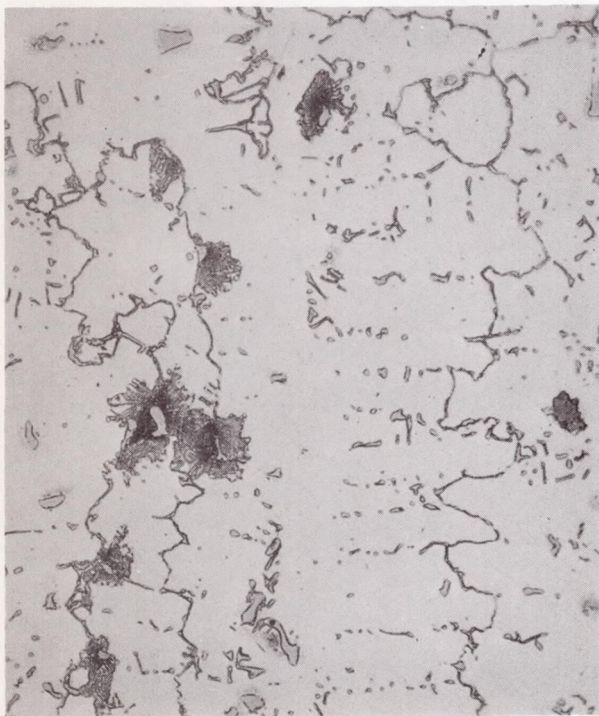
Figure 17. - Continued.



(i) L-605.



(j) X-40.

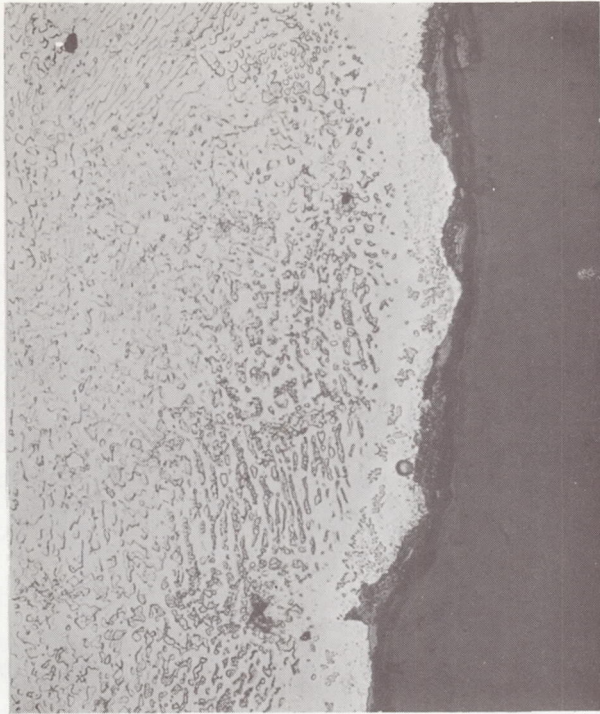


(k) Mar M-509A.

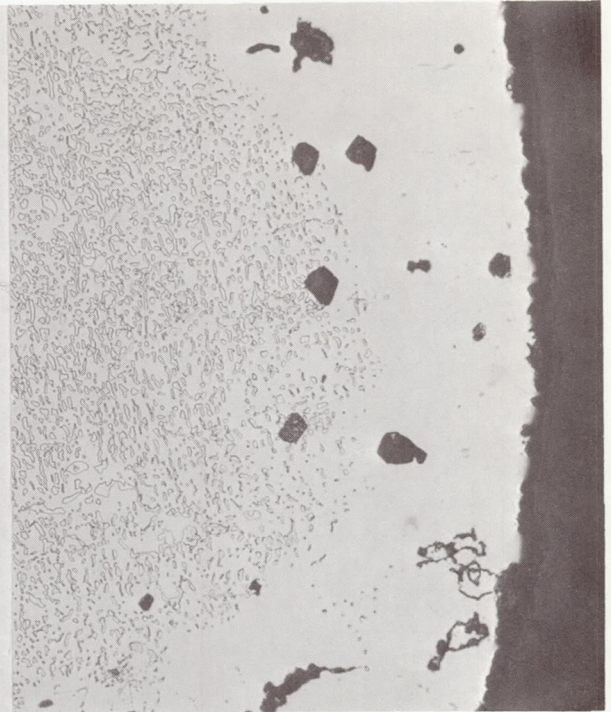


(l) WI-52.

Figure 17. - Concluded.



(a) IN-100.



(b) B-1900.



(c) TAZ-8A.



(d) TD-NiCr (unetched).

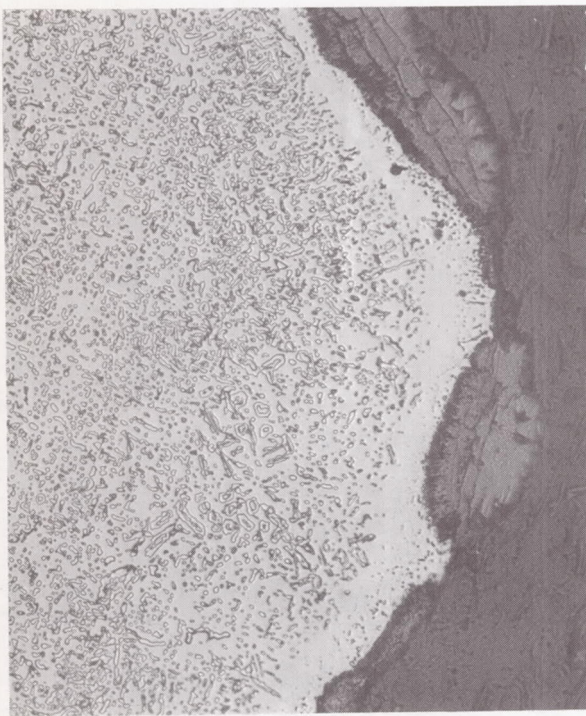
Figure 18. - Microstructures of materials after exposure to standard cycle for 100 hours at 2000° F (1093° C). X250.



(e) Hastelloy X.



(f) Mar M-200 (equiaxed).



(g) Mar M-200 (directionally solidified).

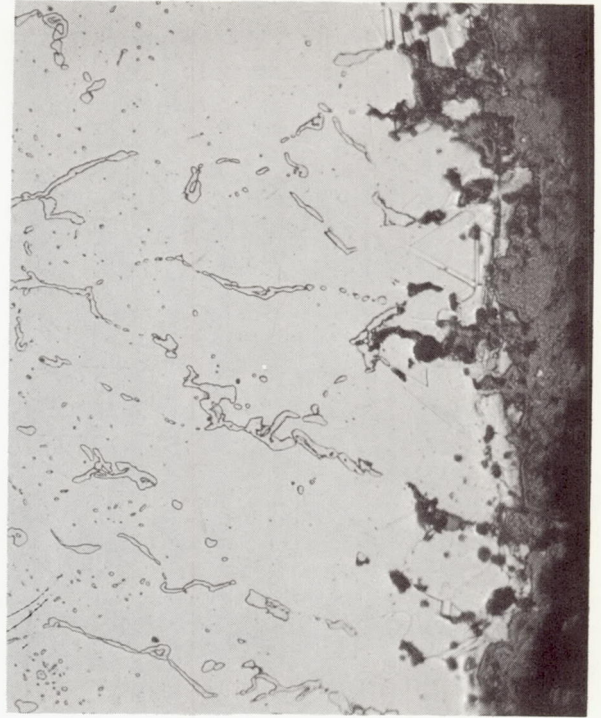


(h) Mar M-200 (single grain).

Figure 18. - Continued.



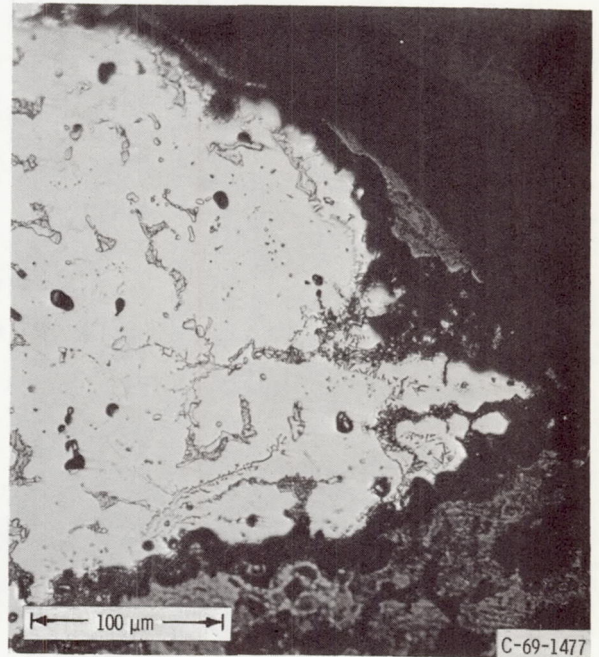
(i) L-605 (1900° F (1038° C)).



(j) X-40.

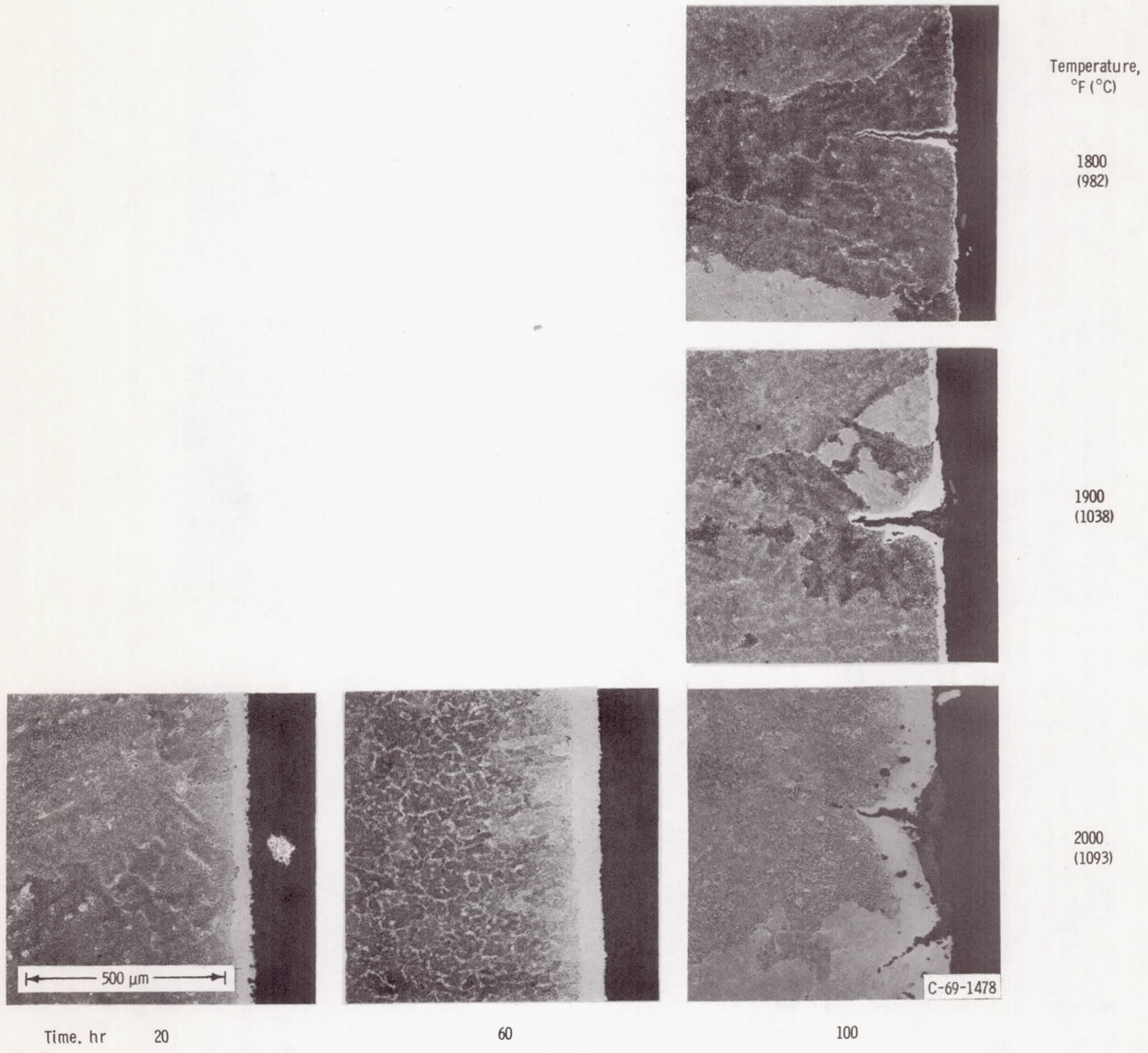


(k) Mar M-509A.



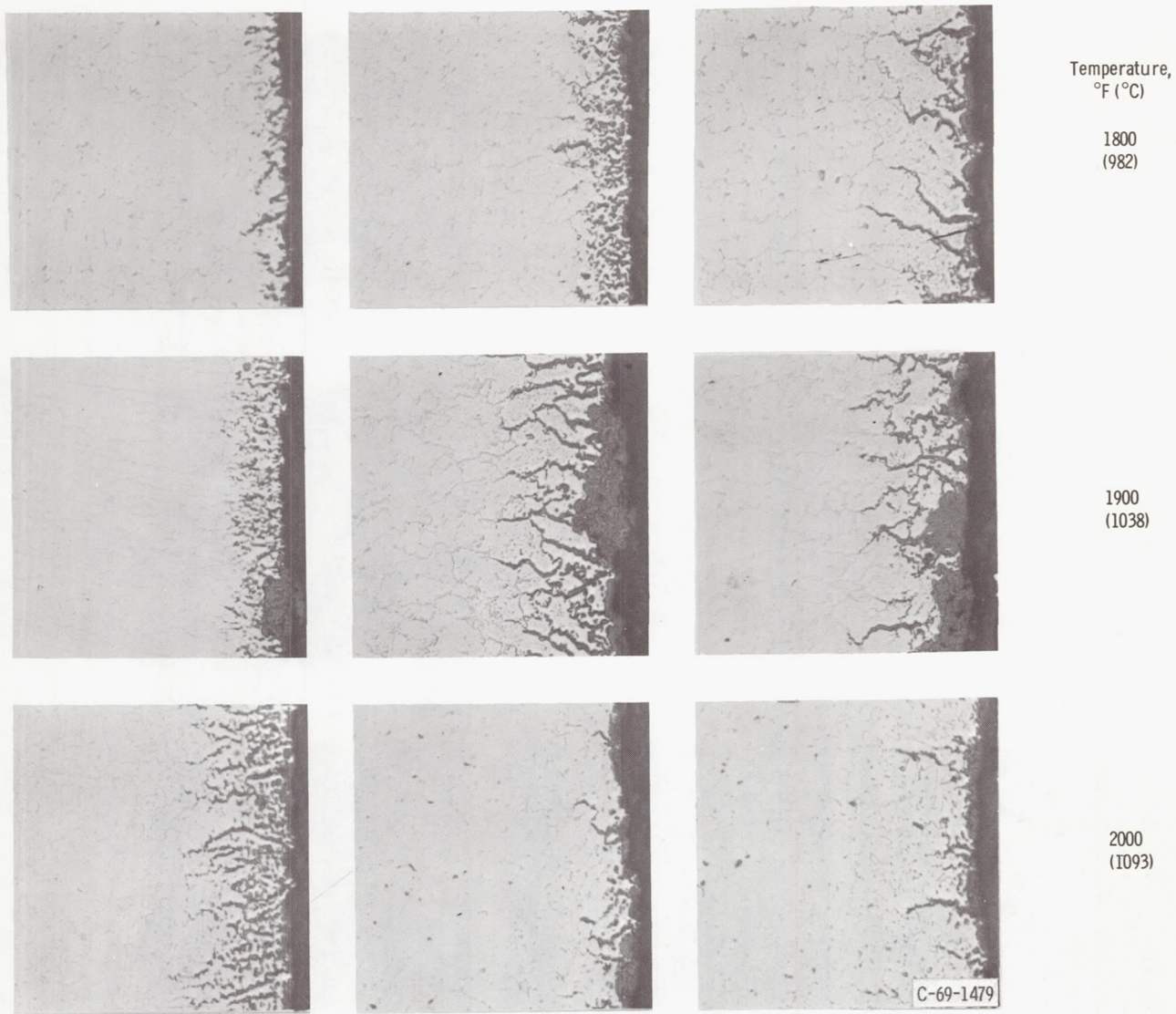
(l) WI-52.

Figure 18. - Concluded.



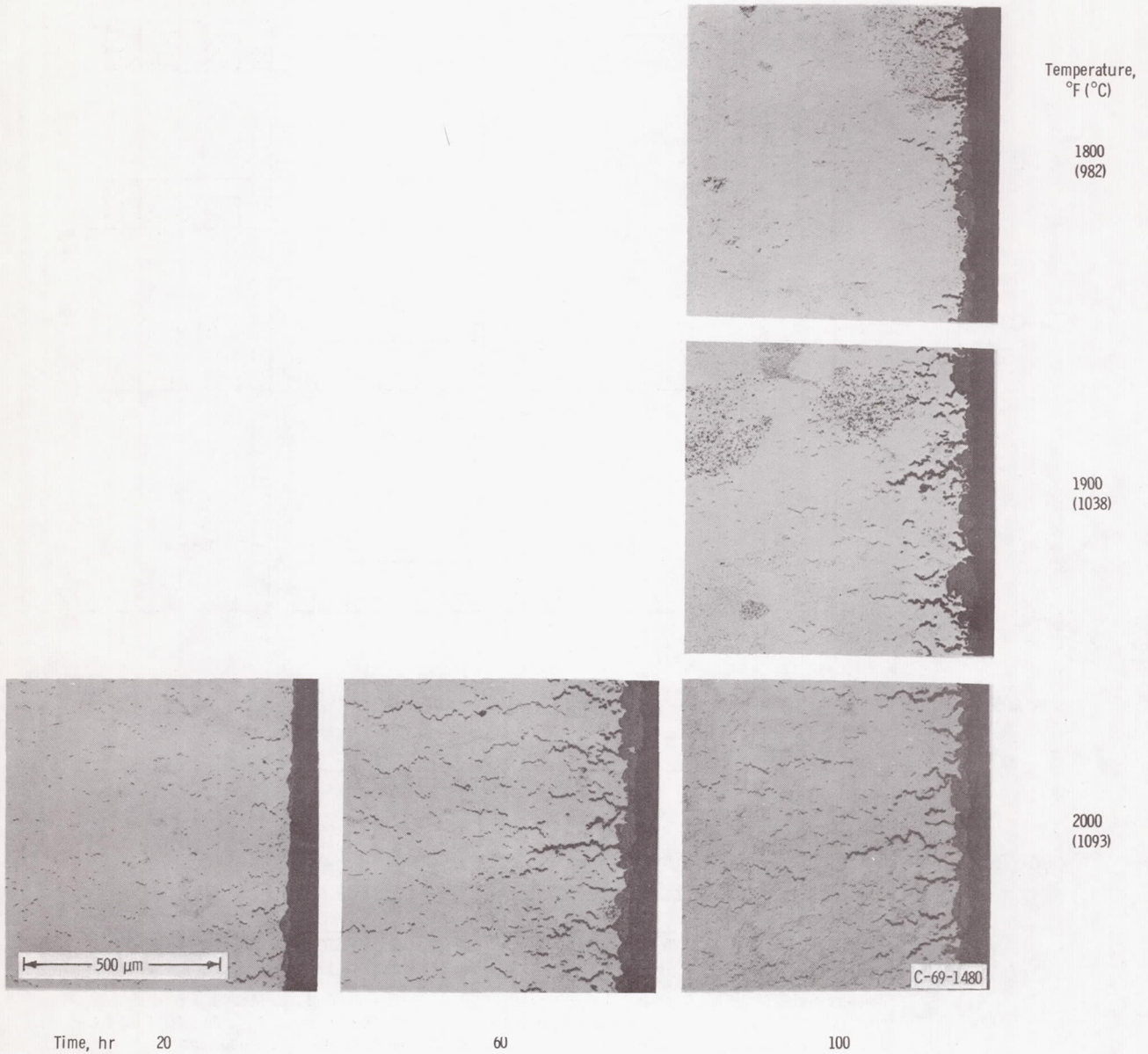
(a) B-1900.

Figure 19. - Specimens after exposure for various times and temperatures using standard cycle.



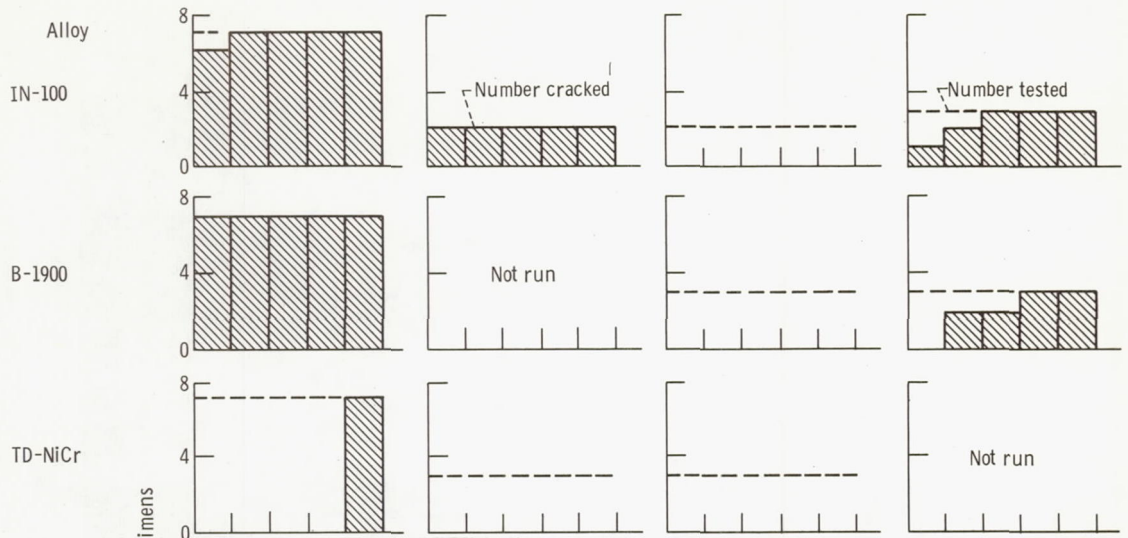
(b) Mar M-509A.

Figure 19. - Continued.

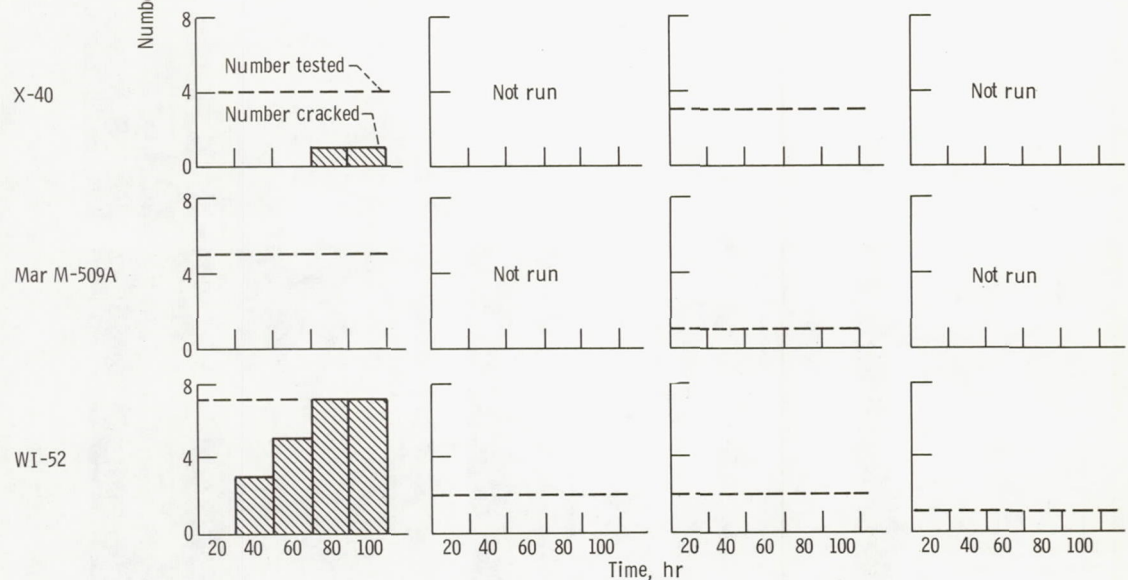


(c) TD-NiCr.

Figure 19. - Concluded.



(a) Nickel base alloys.



Standard cycle: Mach 1; forced-air cool,  $T_{max}$  to room temperature; 1-hour cycle

Mach 0.7; forced air cool,  $T_{max}$  to room temperature; 1-hour cycle

Mach 1; free-air cool,  $T_{max}$  to room temperature; approximately 10-hour cycle

Mach 1; forced-air cool,  $T_{max}$  to 1200° F (649° C); 1-hour cycle

(b) Cobalt base alloys.

Figure 20. - Effect of operating conditions on thermal fatigue cracking of materials at maximum cycle temperature  $T_{max}$  of 2000° F (1093° C).